Cryogenic Heat Switch

A Senior Design Project

Submitted to the Faculty of the

Department of Mechanical Engineering
California Polytechnic State University
San Luis Obispo

In Partial Fulfillment
of the Requirements for the Degree
Mechanical Engineering, Bachelor of Science

Associates:
Daniel Brodkey
Esteban Ruiz
Cristal Vasquez

Date: June 4, 2012

Statement of Disclaimer

Since this project is a result of a class assignment, it has been graded and accepted as fulfillment of the course requirements. Acceptance does not imply technical accuracy or reliability. Any use of information in this report is done at the risk of the user. These risks may include catastrophic failure of the device or infringement of patent or copyright laws. California Polytechnic State University at San Luis Obispo and its staff cannot be held liable for any use or misuse of the project.

June 4, 2012

Team Boreas
1 Grand Avenue
San Luis Obispo, CA 93405

Professor Mohammad Noori
Mechanical Engineering Department
California Polytechnic State University
San Luis Obispo, CA 93405

Dear Professor Noori:

Attached is a copy of the Senior Project report: Development of a conceptual design for a cryogenic heat switch, for the Jet Propulsion Laboratory.

Sincerely,

Team Boreas

Distribution:
Professor Joseph D. Mello: 1 copy

June 4, 2012

Team Boreas
1 Grand Avenue
San Luis Obispo, CA 93405

Eugenio Urquiza, Ph.D.
Cryogenic Systems Engineering
Jet Propulsion Laboratory
Pasadena, CA 91109

Dear Mr. Urquiza:

Attached is a copy of the Senior Project report: Development of a conceptual design for a cryogenic heat switch, for the Jet Propulsion Laboratory.

Sincerely,

Team Boreas

Distribution:
Supervisor Jose I. Rodriguez: 1 copy

Contents

I. Table of Figures

II. Abstract

A prototype cryogenic heat switch capable of transferring heat at cryogenic temperatures, while decoupling to prevent irreversible heat damage and minimizing parasitic heat loads, is to be developed for the Jet Propulsion Laboratory. Various material properties and cryogenic heat transfer processes will be investigated to determine the best solution for this project. A working proof of concept model will be constructed that may eventually be integrated onto a spacecraft's passive cooler systems to protect them from the irradiation emitted by the sun, from the albedo of planets, and other malicious heat sources.

III. Introduction

The Jet Propulsion Laboratory (JPL) has issued this project to develop a prototype cryogenic heat switch capable of transferring heat at cryogenic temperatures. Cryogenic heat switches have several potential uses in space application. They are capable of minimizing parasitic losses from an "OFF" cryocooler in a redundant cryocooler system, as well as decouple from the cryoradiator when irradiated by the sun, or albedo of planets. What made this project extremely challenging is that material properties at cryogenic temperatures are convoluted, esoteric, and highly non-linear.

The goal of this project was to design a prototype cryogenic heat switch that is more reliable and efficient than the current state of the art designs. Extensive research led to the design and building of a conceptual prototype that was tested as a proof of concept. The initial step was to research the topics of interest in order to come up with an innovative and feasible (promising) design. Further research and analysis have been done to verify it will meet the requirements. The prototype has been built and tested in standard pressure and temperature.

Testing and analysis has proven validity of the design and the results have been presented to the JPL group that supported this project so that they may choose to implement it on their passive cooler systems. This prototype may be used by JPL and possibly other space agencies, since it is designed to protect passive coolers from excess heat due to irradiation of the sun, albedo from the planets, and other malicious heat sources. Furthermore, most spacecraft systems have passive coolers and this process is widely used.

In the search for a new conceptual design of a cryogenic heat switch for JPL, two unique solutions initially seemed feasible. The activation mechanism was developed through a systems engineering approach by first understanding the requirements, physical system and environment. Such an approach helped to consolidate the designs options and clarify parameters.

A. Objective

At the completion of this project a conceptual heat switch prototype will be tested for proof of concept. This conceptual prototype will be applicable to various space applications and conducive to several

design implementations. Furthermore, the conceptual model will provide an efficient means of transferring heat in the “ON” (closed) state, reliable “ON/OFF” switching capabilities, while mitigating parasitic heat losses in the “OFF” (open) state.

Implementing a system engineering approach to this design has facilitated a better understanding of this difficult challenge and has assisted in the development of conceptual models. It has promoted conceptualizing various scenarios, understanding the primary concerns, and subsequently optimizing for such cases. Furthermore, understanding the primary requirements and specifications helped establish certain design considerations.

Requirements:

- Low-outgassing materials (Vacuum Pressure < 1X 10E-4 torr)
- Off Conductance < .5mW/K
- On Conductance > 100mW/K
- Closed from 100K-300K
- Power Dissipation < 20 mW
- Lifetime > 5 yrs
- Lifetime > 100 cycles
- Conducts only heat not electricity
- Needs to couple and decouple between cryocooler and detector

Preferences:

- Passive system
- No moving parts
- Small in size

Environmental Conditions:

- T_{∞}= 293K (temperature of electronics surrounding the switch)
- $T_{Cold\ Space}$= 2.7K (never 0K because of microwave background radiation)
- Solar Irradiance at 1 AU from the sun is ~1380 W/m^2

Purpose:

- Couple/De-couple from a failed cryocooler to minimize parasitic heat losses. (See figure 1)
- Couple/De-couple from a cryocooler if/when irradiated by the sun or other malicious heat sources. (See figure 2)
- Couple/De-couple from a redundant cryocooler to minimize parasitic heat losses. (See figure 3)
- Detector is cooled (anywhere from 5K to 100K, we will assume this heat switch is for a detector with a 100K operational temperature) to get precise wavelength measurements by removing IR radiation
- Detector is heated (to about 293K) to decontaminate itself (or to boil off any ice water that may have accumulated on the detector)

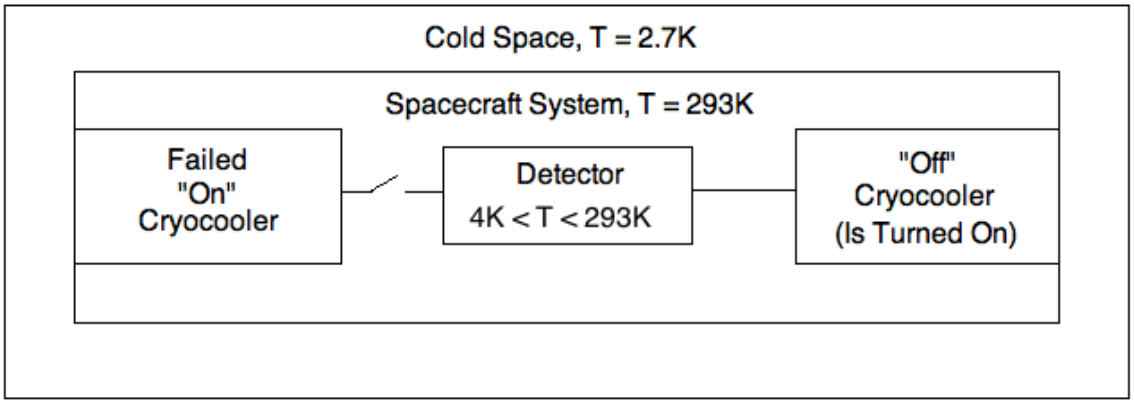

Figure 1. System diagram of heat switch with a failed cryocooler.

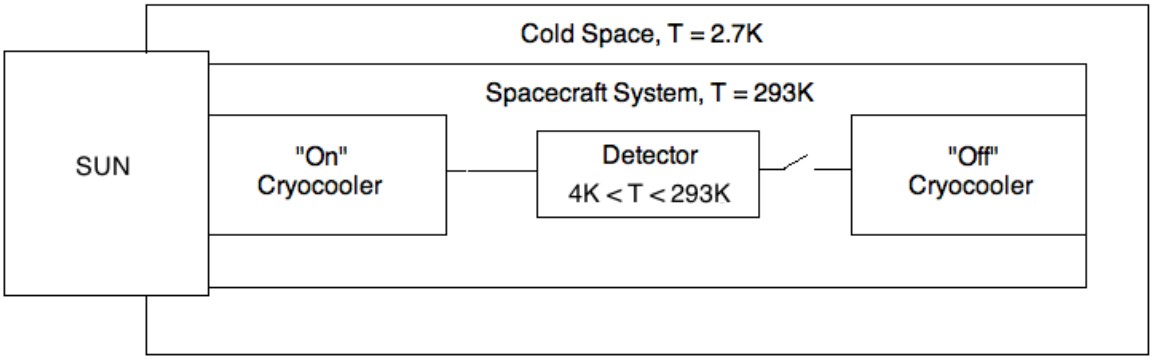

Figure 2. System diagram of heat switch with cryocooler being irradiated by the sun.

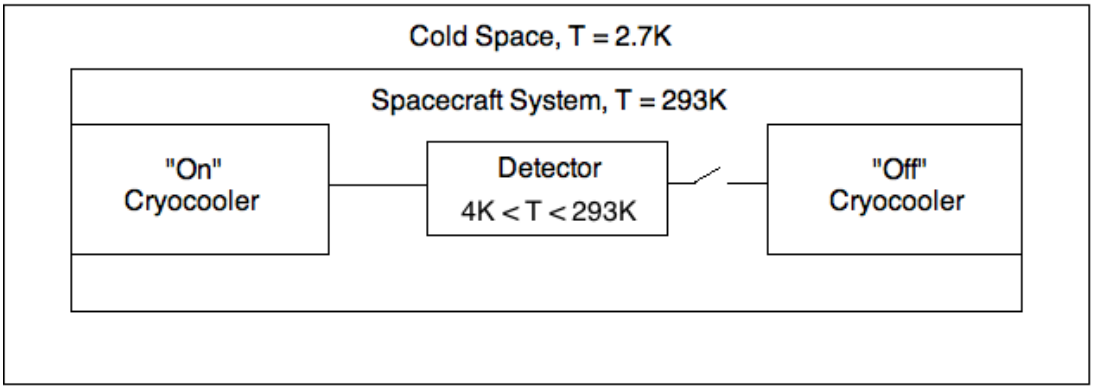

Figure 3. System diagram of a heat switch with the cryocooler cooling the detector to its operating temperature.

In order to show compliance of these requirements, a thorough analysis has been completed as well as testing for proof of concept for the actuation method. The heat conductance ratio between the “ON” and “OFF” states have been calculated as well as the actual temperature at which the states switch.

IV. Background and Literature Review

In space applications, heat transfer is a critical parameter to the function, reliability, and overall life of any object in space. Depending on the objects location relative to the earth, sun, and other stellar bodies, it will experience drastic temperature changes. Electrical devices and other various components are sensitive to such drastic temperature variations, which may impede their functionality and need to be maintained at relatively constant temperatures. Furthermore, the operating temperatures for many of these devices are within a range of 20K to 150K. This range is better known as the cryogenic temperature region.

Cryogenics is a relatively new field of study that originated at the turn of the 20th century. In essence, this term describes the study of extremely low temperatures and encompasses a wide array of subjects and fields of study. Initially, the field of cryogenics was dominated by physicists who developed the methods of obtaining such low temperatures and tested the behavior of various elements at these conditions [1]. However, as the means for obtaining and maintaining cryogenic conditions became more practical, engineers began exploring its potential with the hopes of applying this new knowledge.

Physical properties of matter such as conductance and heat capacity behave queerly at cryogenic temperatures. Furthermore, many of these properties are highly nonlinear and become functions of temperature [2].

As satellites or other objects in space become irradiated (e.g. the sun) the same methods that keep components cool in effect transform into heaters. To maintain the integrity of the space systems this malignant heating effect must be controlled and limited. Furthermore, the uses of redundant cryocooling systems require a means of switching between coolers if one fails. In order to save precious power in space, the mitigation of parasitic heat losses is crucial. Currently, JPL use room temperature heat switches in various space applications to turn heat transfer “ON” and “OFF” from different components. At around temperatures below 300K, the switch will be turned “ON” and have a heat conductance of 100mW/K and above 300K the switch will be “OFF”, which in theory completely mitigates heat transfer.

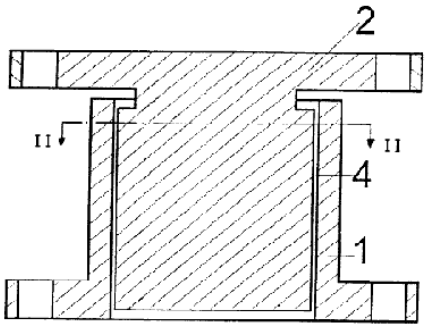

Figure 4. COT Heat Switch.

Currently, several different concepts have been employed to create a cryogenic heat switch. One of the most elegant and “simple” methods utilizes a material’s coefficient of thermal expansion (CTE). At the low operating temperatures, two concentric cylinders make physical contact and thereby allow for heat

transfer. With higher temperatures the materials begin to expand and open up a physical gap that drastically inhibits the transfer of heat. This type of heat switch is not designed for cryogenic temperatures and only work at or above room temperature. Figure 4 above demonstrates this concept [7]. In addition, other designs utilize the thermal conductance of gases in what are called Gas-Gap Heat switches. In operating conditions, a body is filled with a conductive gas and heat is allowed to pass through the switch. However, as the temperature rises gas is evacuated from the body and inhibits heat transfer. Furthermore, heat transfer can not only be shut off but controlled by pressure, making heat transfer a function of pressure as seen below in figure 5.

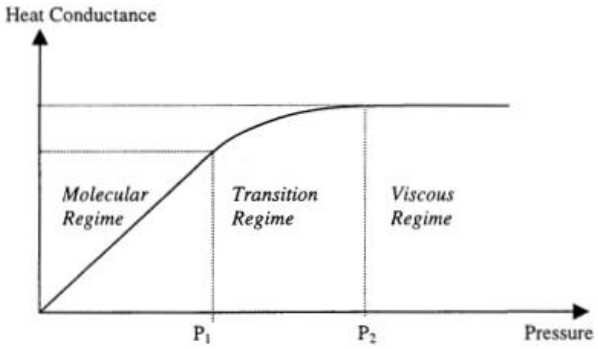

Figure 1: Heat conductance versus pressure.

Figure 5. Heat conductance versus pressure.

The schematic and thermal circuit for this design developed by JPL is shown below in Figure 6. This design is advantageous due to the high "ON/OFF" ratio of 1000 [5].

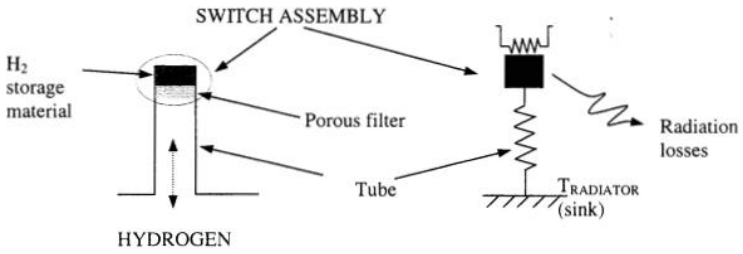

Figure 6. Schematic and equivalent thermal circuit of the gas gap heat.

In addition, further research provides a good overview of the field of cryogenics and its origins. Several interesting physical properties were unearthed such as liquid oxygen's magnetic properties [1]. Another text, *Heat Transfer at Low Temperatures,* edited by Walter Frost, Plenum Press, New York and London, 1975 provides a detailed study of the behavior of heat transfer at cryogenic temperatures. Extensive research on conductive and convective heat transfer through metals, composites, and fluids is narrated [2].

Novel and exotic materials were researched including shape memory alloys (SMAs), ferromagnetic materials, phase change materials, bi-metallics, and piezo-electrics. Out of these SMAs, ferromagnets, and phase changing materials were entertained. Much time had been devoted to the physical characteristics of the materials in order to determine the possibilities for their use in a cryogenic heat

switch. SMAs are brilliant alloys capable of remembering an original configuration based on temperature memory; SMAs undergo deformation, or shape change, and revert back to the original shape at the transformation temperature [3]. Phase changing materials, such as paraffin wax, undergo large volume expansion during phase change. Ferromagnetism is the study by which certain materials form permanent magnets. Ferromagnetism is the strongest type of magnetism and it is characterized as having all of its magnetic ions adding a positive contribution to the net magnetization. Ferromagnetic compounds have what is called a curie temperature; below this temperature the compound exhibits a spontaneous magnetization and above this temperature it ceases its magnetization [4].

In the investigation to model the heat path through the switch, it was discovered that the interfaces between all materials experience a thermal resistance. There is a temperature drop between two interfaces due to microscopic imperfections known as interstitial gaps. For most cases, this thermal resistance is ignored as the atmosphere offsets those imperfections by filling in any gaps between the two interfaces. In space, there is no atmosphere so the thermal resistance has to be accounted for. Modeling the thermal contact resistance (TCR) proved to be highly nonlinear and convoluted. It was found that TCRs are a function of multiple variables such as contact pressure, surface roughness, surface cleanliness, surface flatness, etc. Multiple models were found and expanded upon below in analysis section.

V. Design Development

Through extensive research into various physical properties of several materials and generating initial conceptual models, two initial materials have been identified for use in probable methods of actuation: shape memory alloys (SMA) and ferromagnetic materials.

Several types of SMAs such as one and two-way shape memory alloys, ferromagnetic shape memory alloys, and shape memory polymers exist. In this particular application of a cryogenic heat switch, two-way shape memory alloys and ferromagnetic shape memory alloys initially hold the most promise. Through research on shape memory alloys, two-way SMAs and ferromagnetic SMAs proved to be unreliable and difficult to use and manufacture while more is known about one-way SMAs and should prove easier to obtain and work with.

In the case of ferromagnets, two promising materials are dysprosium (Dy), which has a curie temperature of 88K, and gadolinium (Gd), which has a curie temperature of 292K. It may be possible to use Gd to transfer heat at 292K and below, so when above this temperature there will be no conduction across the heat switch. The Gd would be placed so that when magnetized there is contact between the detector and cryocooler and when it is not magnetized there is no contact. This would protect the detector and the cryocoolers from being overheated due to irradiation from the sun or other malicious heat sources. Dysprosium could be used if an application required actuation in cryogenic temperatures because of its low curie temperature

A. Designs Overview

The team has narrowed the initial conceptual designs down to two designs based on actuation method. These actuation methods are different and unique, and employ exotic materials whose data is obtained from manufacturers, various research papers in their respective fields, and testing of the materials. These designs each hold promise as analysis and initial testing continues.

The first actuation method uses ferromagnets to actuate the switch “ON” and “OFF”. As seen in figure 7 there are two magnets, two thermal straps, one highly conductive material (HCM), and one spring assembly. In the “ON” state, the cryocooler keeps the top magnet cool increasing the strength of its magnetic field bringing the magnets into contact and subsequently stretching the spring. As the cooler heats up, it will also heat up the magnet weakening its force. The spring force will overpower the magnetic force as the magnetic force weakens thermally, delinking the thermal straps from the cooler. The HCM helps keep an even pressure through the full contact area and helps stabilize the heat switch.

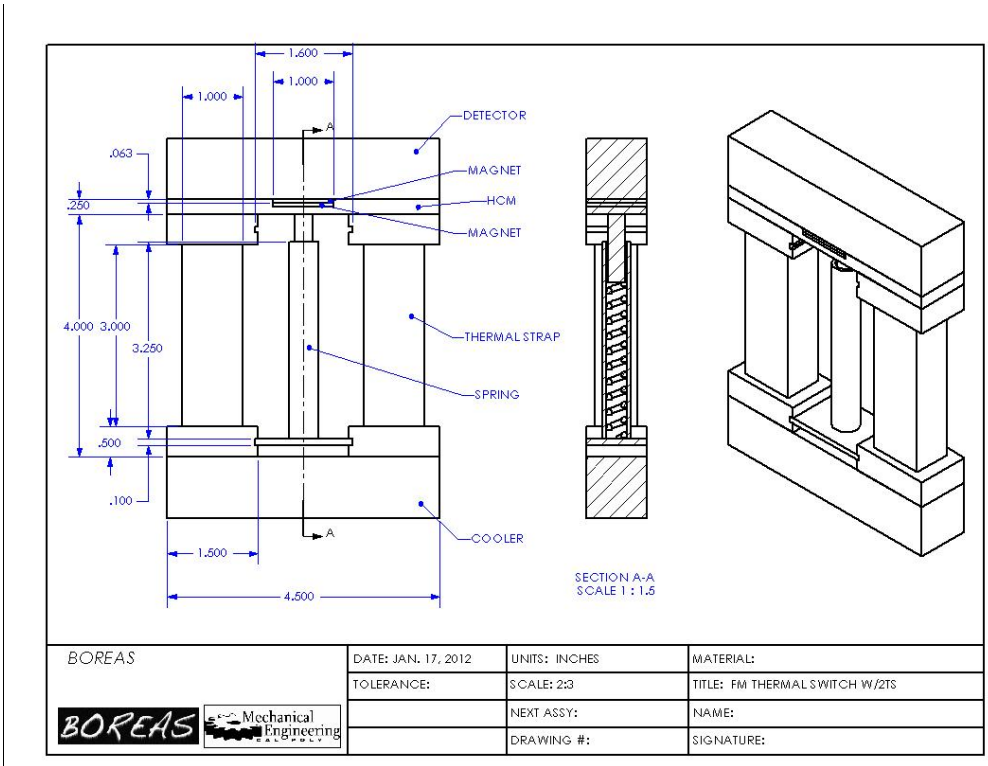

Figure 7. Draft model of ferromagnet heat switch.

In the original design of the ferromagnet actuation (See Figure 8), there was only one thermal strap but four magnets. This design presented itself with stability issues and it was redesigned for better stability as shown in Figure 7.

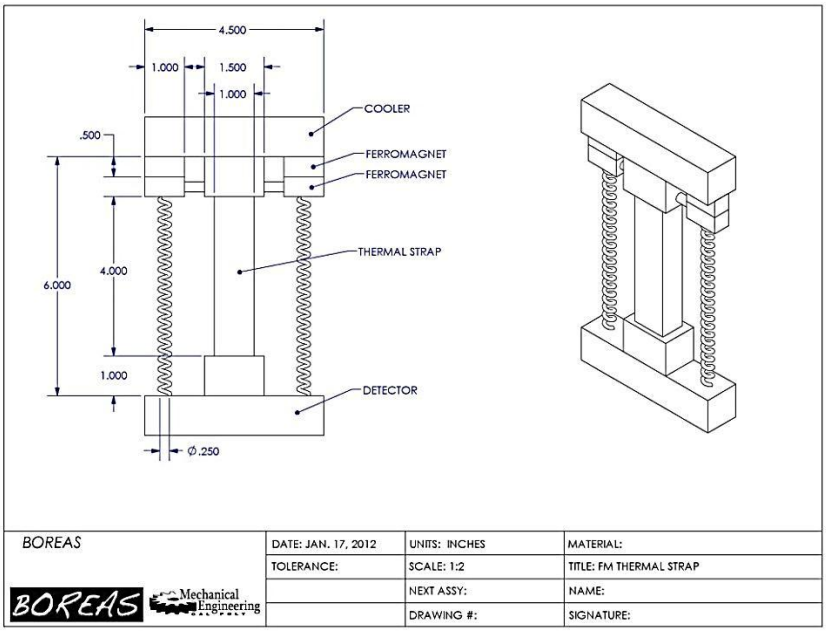

Figure 8. Draft model of original ferromagnet heat switch.

The second actuation method uses one-way shape memory alloys to actuate the switch. As seen in Figure 9 there are two thermal straps, two bundles (i.e. multiple wires tied together in parallel) of wire SMAs, and one spring. In the "ON" state, the spring applies a compressive force to the conducting materials while the SMA is in a stretched position with a martensitic structure. As the cooler heats up the SMA, the SMA transforms into an austenitic structure reverting to its original retracted position by further compressing the spring and pulling the highly conductive material away from the detector, actuating the device into its "OFF" state.

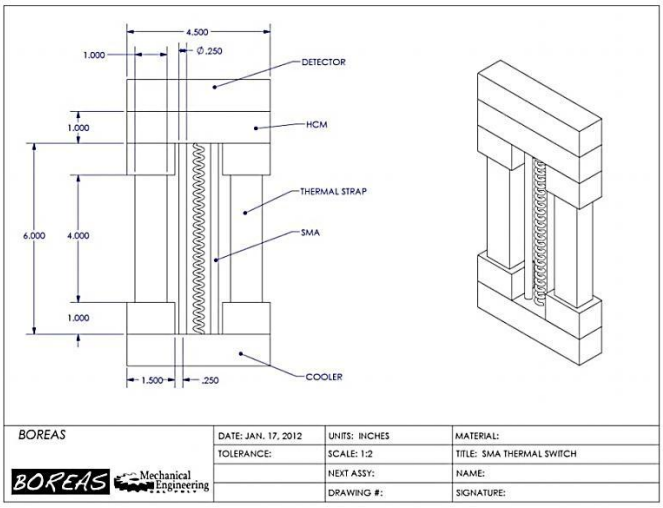

Figure 9. Draft model of SMA heat switch.

In a different iteration of the SMA actuation, the SMA is thermally decoupled from the HCM to minimize parasitic heat losses through the SMA during its actuation (See Figure 10). A low conducting thermal plate would be used to connect the SMAs to the thermal straps. Another HCM was also added to the bottom of the heat switch to give the SMA and the springs something to attach to.

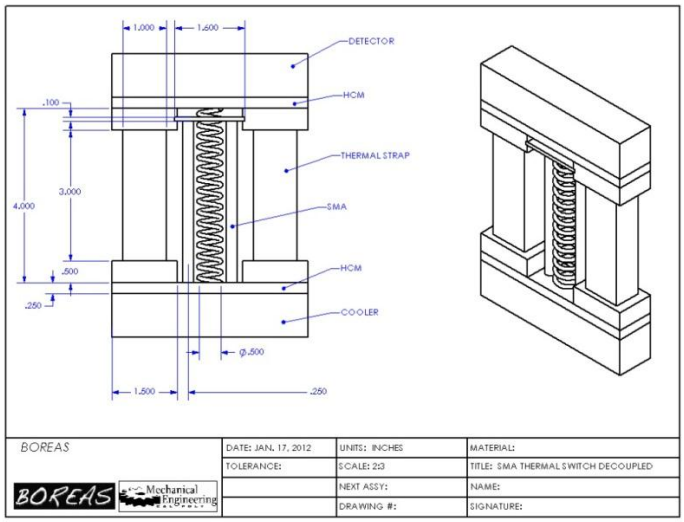

Figure 10. Draft of thermally decoupled SMA heat switch.

Testing of individual methods was done to decide the final actuation method. The magnets responded favorably to thermal cycling as long as its operating temperature was not surpassed. The SMAs proved very difficult to heat up through conduction. Since the SMA is a wire, there is little contact between surfaces a reliable heat path. The SMA's material also has a very low thermal conductivity.

B. Analysis

A thermal EES model has been developed to predict the "ON" and "OFF" conductance values of our two designs. First the "ON" state conductance results will be discussed. In order to correctly model the "ON" state conductance, the thermal contact resistance (TCR) across the two contacting surfaces had to be determined. TCR is a function of pressure, and thus a function of force. Based on preliminary testing of a neodymium ferromagnet a rough estimate of the force they can produce was determined. The SMAs on the other hand had published data that provided pull force for varying diameter nitinol, a type of SMA. With these values of force, pressure was calculated for each design based on assumed geometry. Since there is no way determine the theoretical TCR across these surfaces due to the various imperfections and variable conditions of the materials, empirical correlations from various published journals and textbooks were used instead.

These include estimated values of interfacial conductance, h_i for rough Al-Al in vacuum. TCR is then a function of the interfacial resistance. [10] There is a correlation from a linear interpolation of a SolidWorks table that provides the thermal contact resistance for Al under vacuum for a specific contact pressure. The next correlations came from a linear interpolation of plots with nominal contact pressure vs. thermal contact resistance for A5052 Aluminum alloy for contact of flat surfaces of both rough and

fine finish. [9] The last correlation was a linear interpolation taken from a plot of nominal contact pressure to thermal conductance. [11]

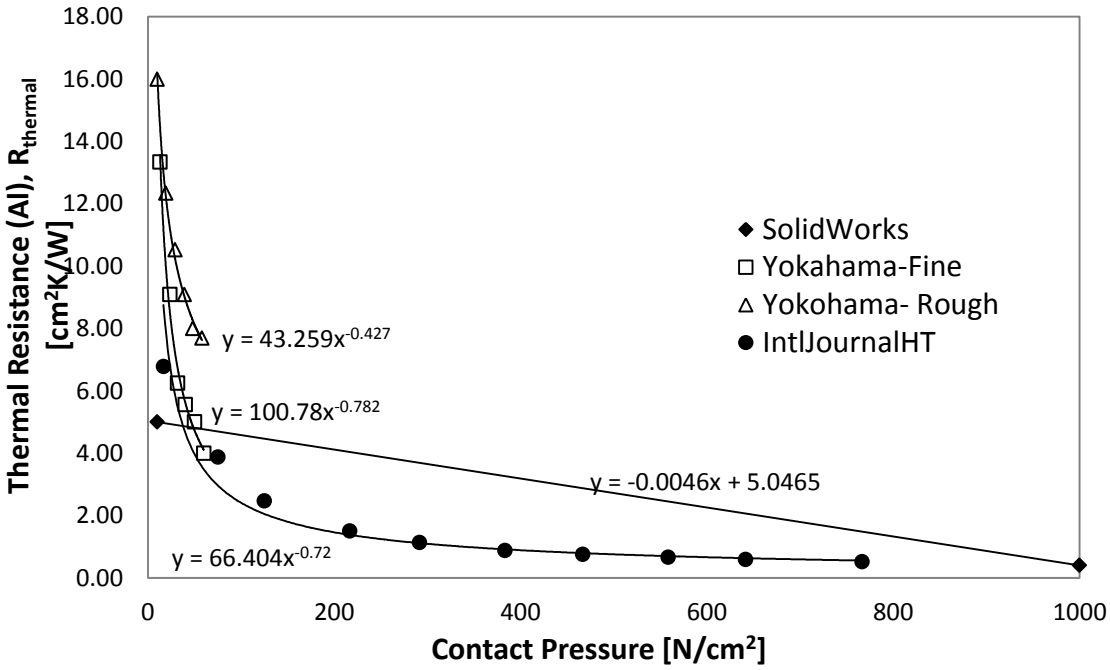

Figure 11. Results for various linear interpolations.

All of our conductance results for the "ON" state ferromagnet design based on 5 different correlations meet the required conductance of 100mW/K, ranging from 248.6mW/K to 1183.0mW/K. They all fall within the same range of values, minus the SolidWorks ($G_{tot,fm,SW}$) data which was about 3 times the average. The average was 405.8mW/K ($G_{tot,avg,fm}$), taken from the average of $G_{tot,fm,JrnlHT}$, $G_{tot,Yoko,rough}$, $G_{tot,Yoko,fine}$, and $G_{tot,fm,Mills}$. (Note: this excludes the SolidWorks model because of inconformity.) These results show that with the assumed geometry and force of the ferromagnet, this design would meet the conductance requirement.

The results for the "ON" state conductance of the SMA design also meet the required conductance value, ranging from 339.5mW/K to 1216.0mW/K. The average of their values excluding the SolidWorks data is 521.1mW/K ($G_{tot,avg,sma}$).

The "OFF" state conductance results are also reasonable, ranging from 0.9mW/k to 1.2mW/K. When compared to the "ON" states average conductance values, the ON/OFF ratio requirement of 100 is met. The "OFF" state conductance across the gap (the two faces that are detached) due to radiation has been calculated as a function of temperature, emissivity, thickness of the gap, and geometry. The radiation across the gap was combined in series with the resistance across the thermal strap for the final overall "OFF" state conductance.

The group also determined the “OFF” state conductance for atmospheric testing which includes the radiation and the conduction terms across the gap due to air at STP. The value of conductance due to the conduction across the gap for the SMA is 3.86mW/K and for the ferromagnet is 34.7mW/K.

Ferromagnets and SMAs were tested for actuation force and actuation temperature. Springs were chosen in accordance to the desired actuation temperature and actuation force. Once springs were chosen a stretched length was determined to pull the magnets apart at the desired temperature range. Fine tuning was completed once the prototype was built to get the needed stretched length of the spring. Analysis is available in appendix E.

C. Preliminary Testing

In order to determine the strength of the neodymium magnets and shape memory alloys as a function of temperature, various pull tests were conducted over a range of temperatures from room temperature to over 100 degrees Celsius. Magnets of several different sizes and thickness were used. Identical pairs of magnets were fastened using JB Weld onto pieces of metal and a power resistor was fixed underneath one of the sets to increase the temperature of the magnets. The power resister was rated for 10Ω and 25W.The power resistor was placed into a vice with wooden soft jaws to provide insulation, and the resistor was hooked up to a DC power supply to control power and voltage. The bottom magnet was screwed into the wooden soft jaws to fix both the magnet and resistor. Thermocouples were placed on the magnets and resistor to monitor temperature and verify steady state conditions. The first thermocouple, labeled T1 in figure 12, was placed beside the top magnet to measure its temperature. The second thermocouple, labeled T2, was placed near the resistor, as seen in figure 12, to monitor its temperature. The opposite magnet was placed on top of the fixed magnet, allowed to reach steady state, and then, using a linear force gauge, pulled apart from the magnet in the vice. Figure 12 shows a schematic of the test set up, figure 13 shows the actual test set up, and figure 14 shows the locations of the thermocouples.

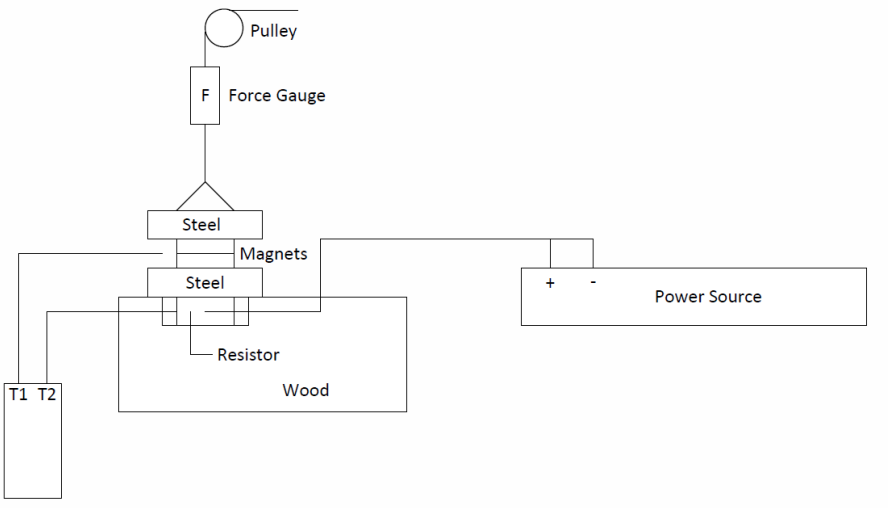

Figure 12. Schematic of test setup for neodymium magnets.

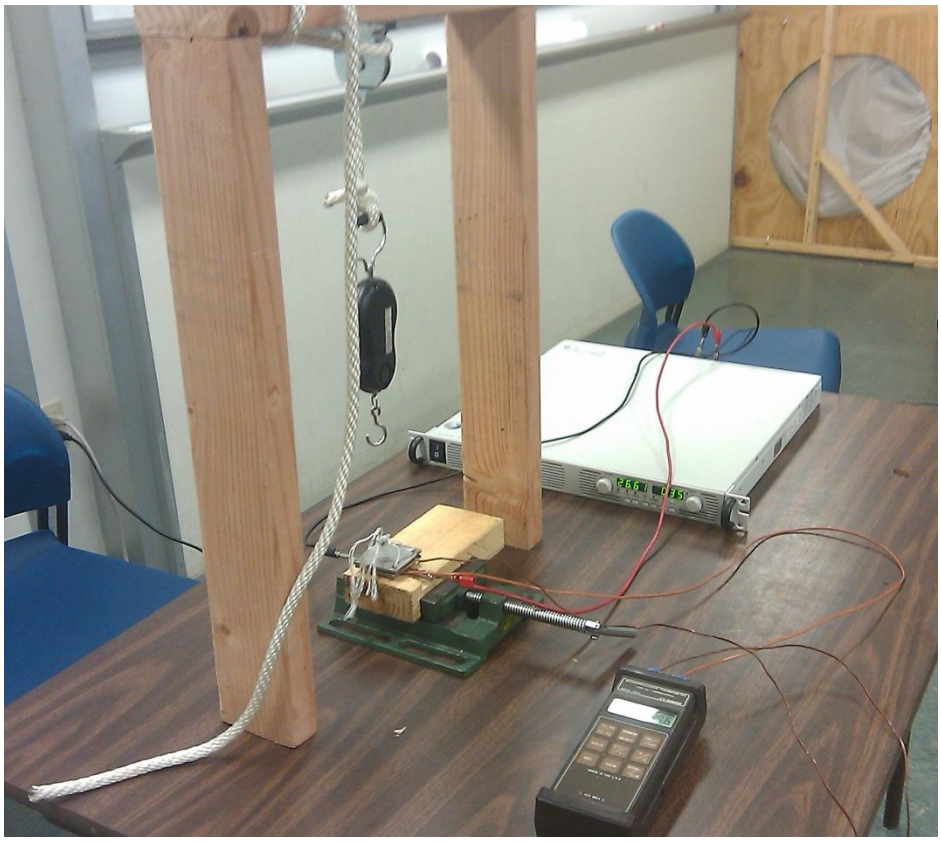

Figure 13. Actual test set up used to test magnet's temperature dependence.

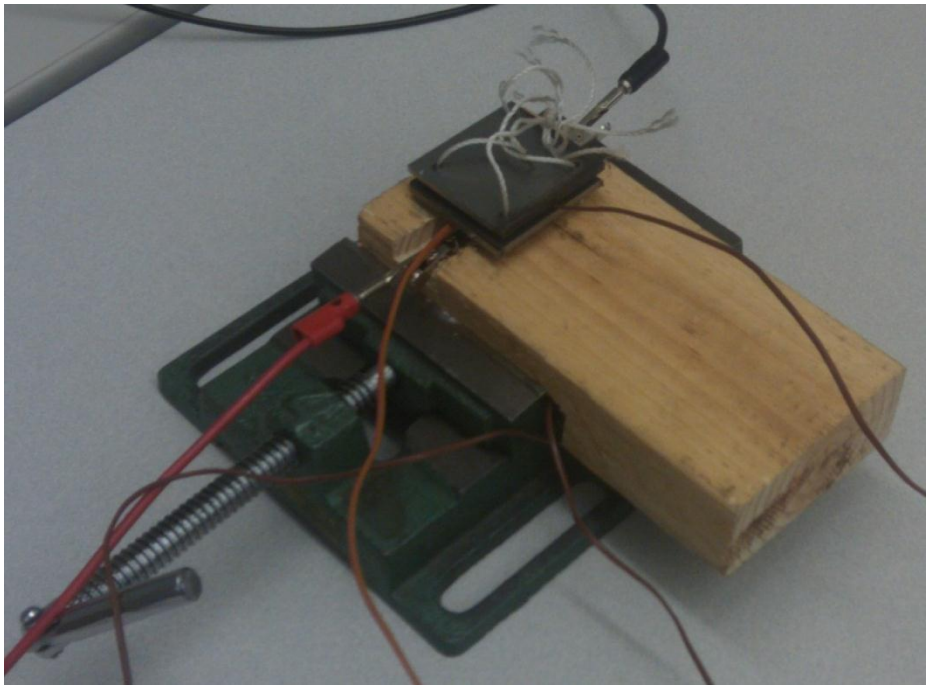

Figure 14. Wooden soft jaw and thermocouples.

Implementing a pulley allowed for more control over the rate of pull as well as keeping the direction of force application constant. Temperature values were increased from roughly 10°C to 100°C in 20 degree increments, with several readings of force data obtained at each temperature value.

The first test was conducted on ¾" x ¾" x 1/16" neodymium magnets which were fastened with epoxy onto 2X2 inch pieces of steel. The magnets were heated up to a temperature of about 80°C. The magnets were tested for force using a pull test three times. The magnets were then allowed to cool down to about 70°C. Magnetic force was then measured again. This was continued at increments of 10°C until it reached room temperature. For the first set of tests, the magnets were not tested for temperatures below room temperature. The force was divided by the magnet's area of 0.5625in^2 to obtain the pressure. The pressure versus temperature is plotted below in figure 15. The temperature of the bottom magnet and top magnets are T1 and T2 respectively.

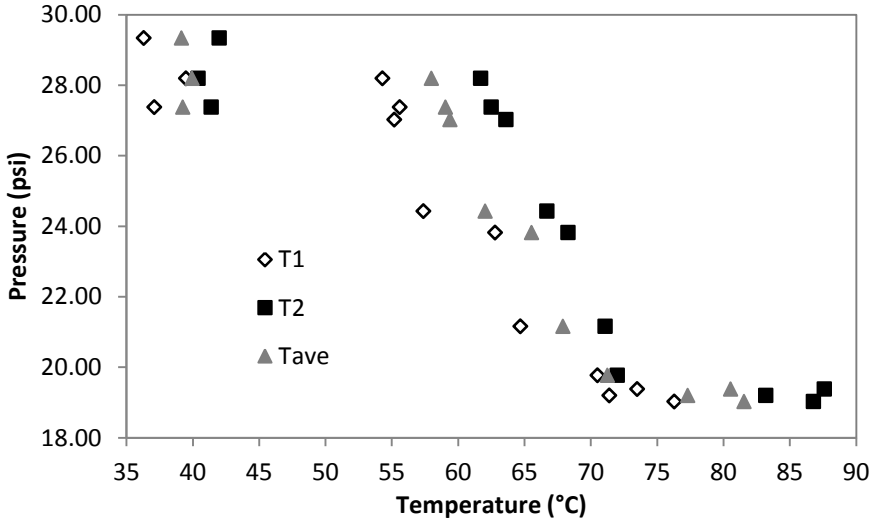

Figure 15. Plot of pressure versus temperature for ¾ x ¾ x 1/16 in neodymium magnets.

A similar process was repeated for smaller magnets with dimensions of 1"x½"x1/32" corresponding with an area of 0.5in^2. These magnets were again attached to 2"x2" pieces of steel, set in the test vice and heated. Testing began at 100°C, and was then backed down to room temperature. Again several data points were taken at each specified temperature. The magnets were then heated again passed its operating range to a bottom magnet temperature (T1) of 160°C and top magnet temperature (T2) of 120°C. Forces continued to decrease as the magnets were pushed beyond their operating limit. The magnets were allowed to cool and were then taken down to near freezing temperatures. This was done by resting a bag of ice on the top plate. The bag of ice cooled the magnets down to near 5°C. However, the force values obtained that were less than that at room temperature which indicated that the magnets underwent irreversible damage and the magnetic field permanently weakened. This is due to the fact that neodymium forms neodymium (III) oxide, which tarnishes the magnet and easily burns in air at 150°C. This did not happen with other test subjects, which validates that it was not the cold temperatures that reduced the strength, but proved that the operating temperature must be

considered to avoid permanent magnetic deformation. Figure 16 displays the effect of temperature on pressure for this specific test.

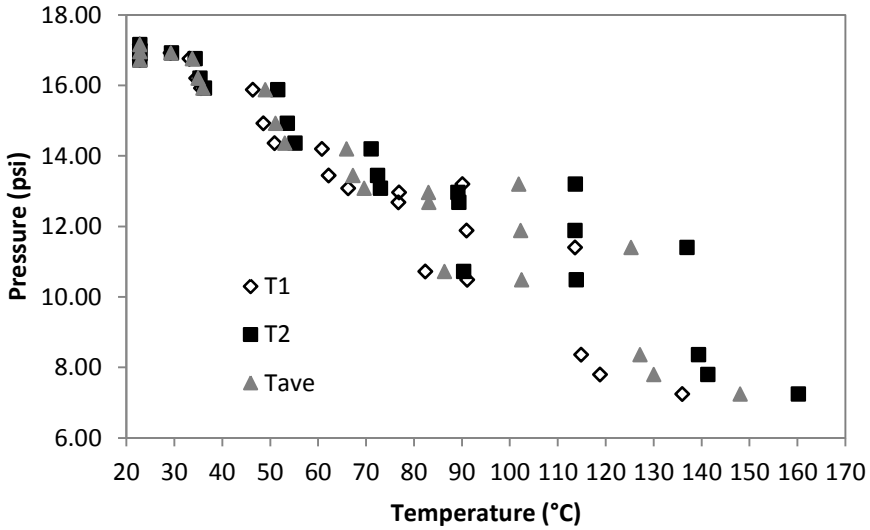

Figure 16. Plot of pressure versus temperature for 1 x ½ x 1/32 in neodymium magnets. Magnets featured irreversible damage beyond 100°C.

Testing was also done on a third magnetic specimen with dimensions of ¾”x3/8”x1/32” to investigate the strength of our smallest magnets and validate the first two tests. Two of these magnets were placed side-by-side on a piece of aluminum, which was done to discover the effect that thickness has on the magnetic strength. With two magnets on each side, the effective area was 0.5625in^2, and equal to that of the first test specimen, however the thickness was decreased by a factor of two. The bottom aluminum piece had dimensions of 2”x2-7/8” and the top 1”x7/8”. Aluminum was used to speed up the rate of heating, obtain closer equilibrium values of the top and bottom magnets, and to better mimic the probable conditions in the final design. On this test, data was collected at lower temperatures first, around 6°C, and were subsequently increased. Force values at low temperatures gave values near room temperature, with only a few values that gave higher force readings. This may be due to inaccuracies in the pull, or that the magnets do not continue to increases much in strength as the temperature is decreased. The aluminum proved to both heat up more quickly but also provided smaller temperature differentials between the two plates. Data was collected up to 60°C when the epoxy then failed. This was not expected because the epoxy had maintained its hold on the bigger magnets, which experienced forces almost double in magnitude. It seems that the epoxy did not bond as well with the aluminum, the coefficient of thermal expansion deteriorated the bond, and/or the nonferrous characteristics of the aluminum did not allow the magnets to magnetically attach thereby increasing the contact with the epoxy. The test was repeated with fresh epoxy and again the epoxy failed. Such results lead to the conclusion that the coefficient of thermal expansion, which is much higher in aluminum than steel, was the cause for the epoxies failure. These characteristics must be considered for implementation of the final design. As such, data was only collected up to 60°C as can be seen in the plot of pressure versus temperature in figure 17.

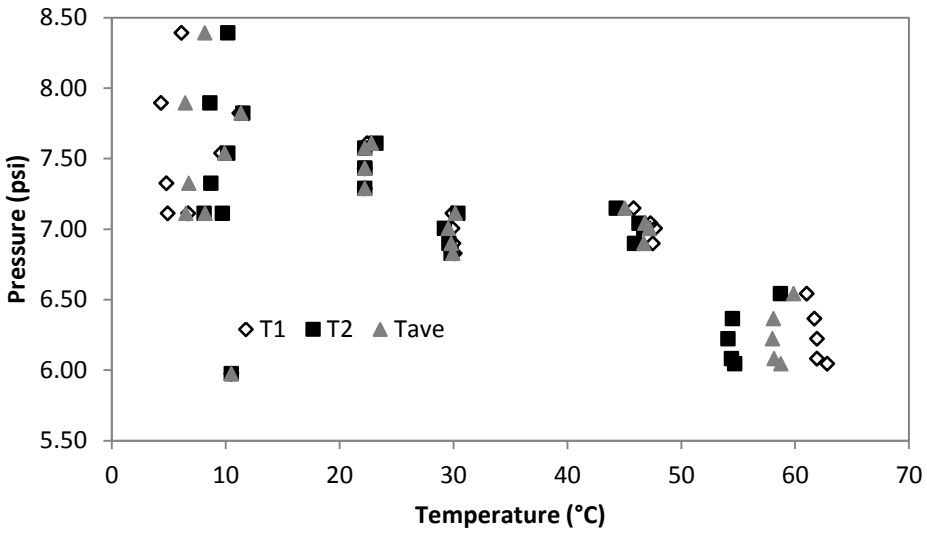

Figure 17. Plot of pressure versus temperature for the pairs of ¾ x 3/8 x 1/32 in neodymium magnets on aluminum plates.

A similar test bed was used when testing the SMAs as seen in figure 18, 19, and 20. Aluminum was used as a test plate along with the same power source, thermocouple reader, force gauge, resistor, and pulley. Two types of SMAs were used: nitinol springs and Flexinol® Muscle Wires®. Flexinol® proper tied could be found in appendix D. A low temperature type 375 was used.

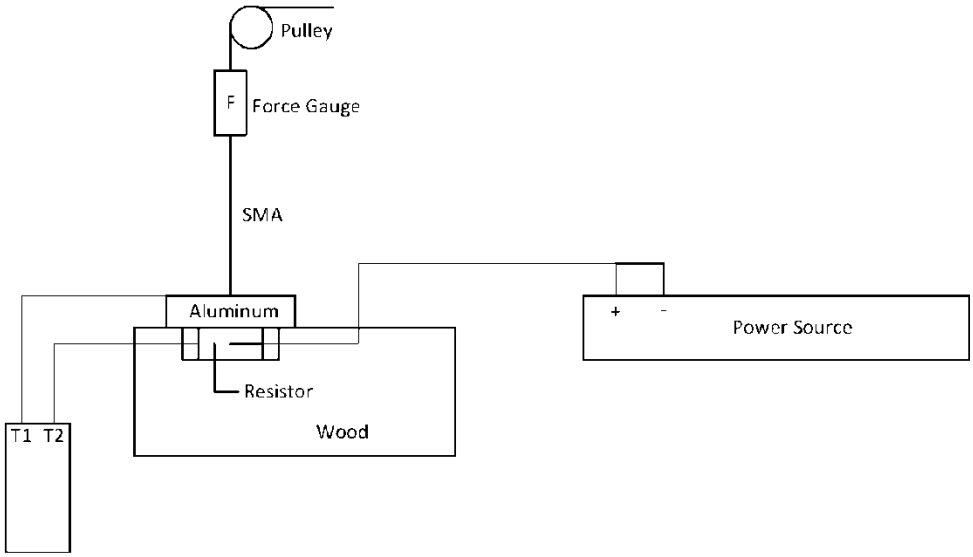

Figure 18. Schematic of test setup for shape memory alloys.

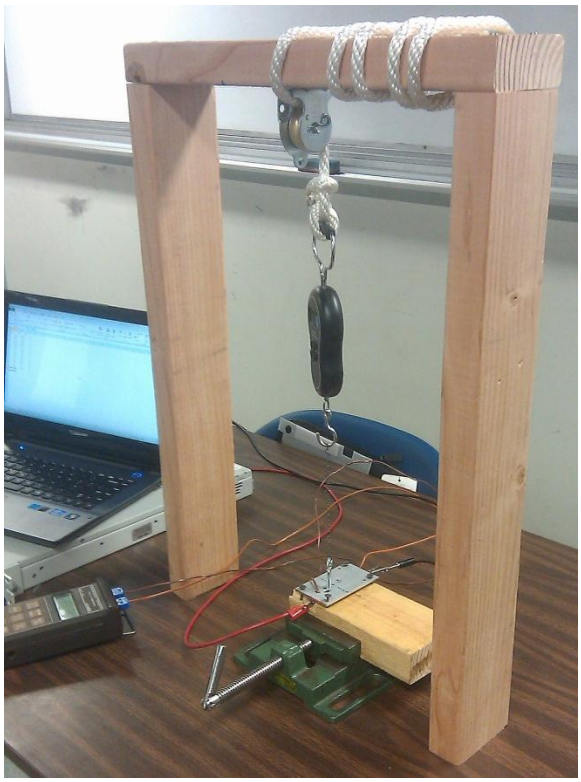

Figure 19. Actual test bed for nitinol spring and Fexinol®.

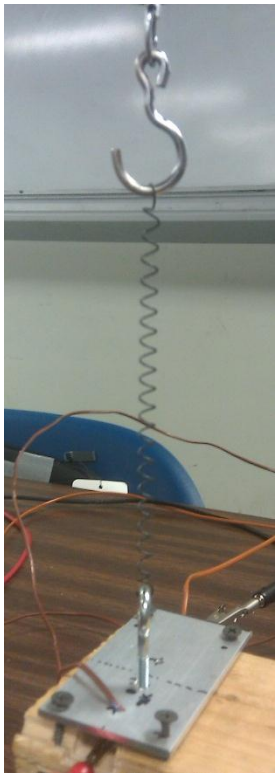

Figure 20. Nitinol spring in set up. Flexinol® wire had similar position.

A nitinol spring was attached to an eye hook. The nitinol spring has a wire diameter of 750µm, could be extended to 14cm and contracted to 29mm, and an actuation temperature of 45-55°C. The power source was turned on to heat up the power resistor and the top plate in an attempt to heat up the spring to actuate. In the first trial, the resistor and top plate were heated to a temperature of 90°C. The spring did not experience any measurable change in shape or force. In the second trial, a heat gun was used to heat up the eye hook. The eye hook reached temperatures of 145°C. The nitinol spring still did not actuate. In the third trial, the heat gun was pointed toward the bottom of the spring, nearest to the aluminum. The spring finally actuated when heated directly and experienced pull forces of about $0.8lb_f$. The spring also only contracted in the area it was being heated. In the final trial, the heat gun was pointed directly at the spring to note the forces it experiences. The spring produced forces of about $3.0lb_f$. The spring would only contract at the point where the heat gun was pointed.

Based off these results, the nitinol spring only actuates when heated directly by the heat gun or when running current through the spring. Even if a heat path was perfected, the nitinol spring ideally only supplies a $3lb_f$ pull force, which is not enough for this application, though this may have been solved by using multiple springs in parallel. The nitinol spring will also have a slow reaction time since its main components, nickel and titanium, are very poor thermal conductors.

After the Nitinol spring trials, Flexinol ® Muscle Wires® were used in a similar test setup. The power source was connected to the power resistor to heat up the aluminum plate. The Flexinol® did not actuate either by heating up the aluminum plate. A heat gun was then used, instead of a power resistor, to heat the aluminum plate to 70°C. Once at 70°C, the heat gun was turned off. Since the Flexinol® was wrapped around the aluminum, it did actuate by direct heating producing a force of $0.16lb_f$. In a second trial, the power source was connected directly to the Flexinol® with 2.5A of current and 4V. The maximum recorded force of the Flexinol® was $0.66lb_f$.

While the Flexinol® did actuate via heat using the heat gun (the Flexinol® was wrapped around the aluminum plate) the forces produced were small. Higher pull forces could be achieved by putting multiple Flexinol® in parallel (i.e. in a bundle). Testing was also stopped because the loads were small and power was needed to fully actuate the Flexinol®. Also, if bundled together to achieve higher loads, the bundle will not heat up uniformly causing more reliability issues.

If the magnets were to be used, the magnets will not be in perfect contact as the experiment assumed. The effects of distance on the magnetic force were measured. This was done using the same equipment for the ferromagnet test as described above. Pieces of paper were placed between the two magnets to increase the space between the magnets. The pieces of paper used measured to be 0.0038” thick. The experiment was conducted in room temperature from zero to eighteen pieces of paper. The data collected is tabulated and graphed below.

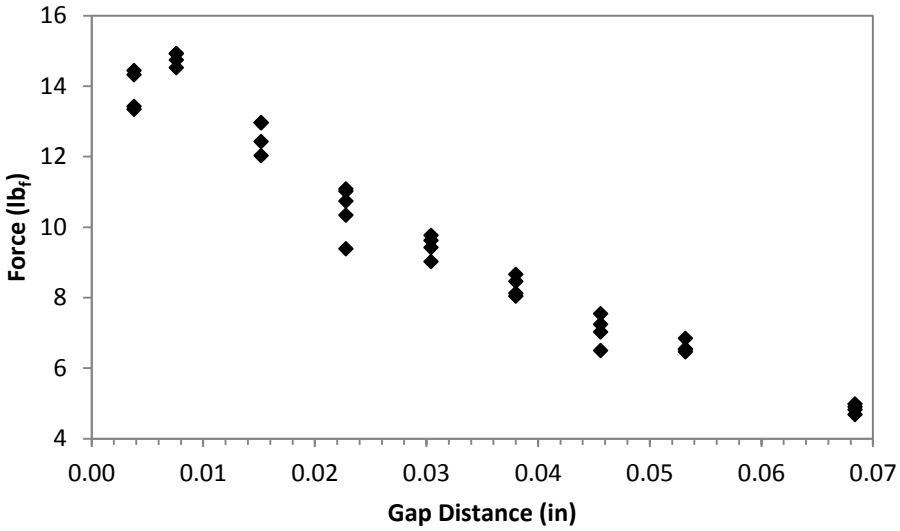

Figure 21. Magnetic force decreases, as magnets are further away from each other.

As was expected, the magnetic force decreases as distance between the magnets increases. It should also be noted that the force drops off significantly over a short distance. Special care will be taken in designing the separation of the magnets in the "OFF" state so they will reactivate.

VI. Final Design

Since SMAs required power to actuate, magnets will be used in the final design of the heat switch. As seen from the test results, the magnets consistently get weaker as temperature begins to increase significantly, as predicted. Hysteresis was also noticed, especially the permanent deformation experienced by the 1"x1/2"x1/32" magnets. Neodymium magnets have a max operating temperature of 80°C which was discovered to have irreversible effects on the magnets if surpassed. As seen from figure 21 above, the gap has been chosen carefully to ensure that when the magnets cool there will be enough force to reactivate the switch.

Final dimensions of the heat switch would be decided based on the application and requirements of the heat switch. Furthermore, different types of magnets would be used depending on application. Dysprosium (Curie temperature of 88K) magnets are suggested if the actuation is desired at cryogenic temperatures. Different materials would also be used depending on application. Aluminum is suggested for its high thermal conductivity and low cost, but copper could be also used if required. Depending on temperature range desired, springs would be chosen accordingly along with the magnets to get the desired actuation temperature. Also, a mechanical device may be required to re-actuate the device once cooled.

The final design is not more clearly defined as it will vary by project, application, and requirements. This project was to prove a new method of actuation. The method of actuation is verified below.

VII. Design Realization

In order to determine the validity of such a magnetic switch design, a conceptual prototype was developed to test magnetic actuation at room temperature. The prototype replicated the characteristics and dimensions of the final designs actuation, while eliminating the main thermal transportation devices by removing thermal straps. This decision was made to reduce complexity and allow for more focused testing on the actuation itself.

Once the basic dimensions where established and materials selected, the design and implementation of incorporating the magnets was addressed. In the first iteration of the design, two neodymium magnets were epoxied onto separate pieces of steel. One was placed at the bottom of the upper support while the other was placed into a channel that was machined out of the steel, as similar to the final design. Because placement and position of the magnets was of paramount importance to their strength and behavior great care needed to be taken with the channels width and depth. To accomplish this task, computer numeric controlled machining (CNC) was used. The program Cam Works enables the ability to define tool paths and machining specifications within Solid Works, and then converts that information to G-Code. Using this program along with the HAAS TM mill located at the Mustang 60 machine shop on the Cal Poly campus, the precise channel was machined. Similarly, to ensure the spring alignment was correct the four tapping holes necessary to attach the actuation springs were machined using the TM mill as well. The precise alignment was necessary to maintain alignment and forces in the vertical direction. Furthermore, the use of threaded holes provides the ability to fine tune the length of the springs and thus the force they provide to set actuation points.

Figure 22. CNC milling process for machining the channel used to house the magnets.

Upon assembly, it became evident that implementing the magnets with the channel design posed several difficulties. Most noticeable was the fact that the magnets were attracted to the inside walls of the channel which made it nearly impossible to maintain proper alignment while setting the epoxy. Additionally, as the epoxy was laid on by hand, the height of each layer was difficult to control which issued variability in the height thus affecting the on state gap distance between the magnets. This gap distance is crucial to the design and has a pivotal role in the magnetic attraction as force decreases with the square of the distance. For these reasons, this design was dropped for testing purposes and the magnet was placed upon the top of the steel block instead. This does not as closely mimic the final design, but for the purposes of validating a proof of concept, proved effective. This modification further simplified the design by eliminating the gap distance in the "ON" state. The reduction of that variable reduced the uncertainty and gave more direct control over the actuation.

The assembled prototype can be seen below in figure 23. Two blocks of wood provide the support for the structure and the attachment point for the various brackets. The brackets located below the actuating block of steel determine the position of the "OFF" state and can be adjusted by the slot in the bracket. Eyelet hooks serve as attachment points for the actuation springs and the treading allow for setting the stretched length of the springs as they can be varied by nuts on the lower half as well as by thread engagement on the upper.

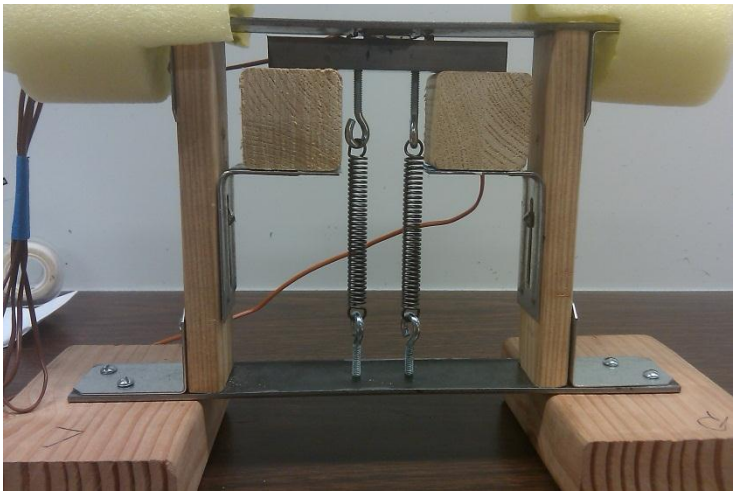

Figure 23. Final prototype used to test magnetic actuation.

VIII. Design Verification Plan

Testing of the prototype was conducted at Cal Poly at standard temperature and pressure. Several tests were conducted to verify that the actuation method is reliable after multiple actuations. A picture of the prototype is located above in figure 23. There is no open channel with the HCM as first designed. Since the HCM was steel, the channel caused misalignment issues due to the magnet being attracted to one side more than the other. The set up shown allows to test for proof of concept but does not allow to check either "ON"/"OFF" ratios nor heat transfer through the HCM. A heat gun was used to quickly heat the device.

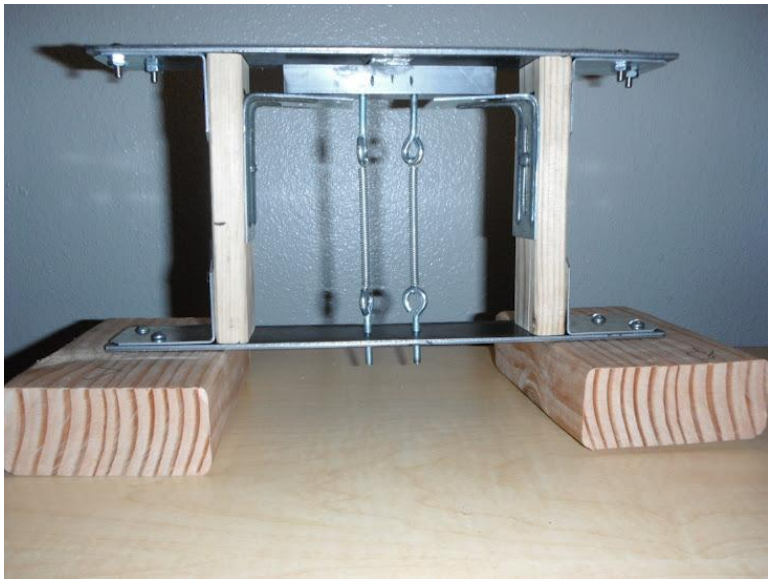

Figure 24. First iteration of proof-of-concept prototype.

Figure 25. Original springs used. Right spring is before deformation, left spring is after deformation.

The first set of testing was done using thin wire springs as pictured in figure 24 and figure 25. The springs were steel with nickel plating, 0.19in diameter, and 1.37in in length. These springs were chosen after performing a pull test to determine their spring constant and the necessary stretched length needed to pull the magnets apart at the desired temperature range. The spring constant measured was $5.5lb_f$/in. This resulted in an elongation of 1in for each spring to have a combined load of $11lb_f$ for actuation around 70°C. After multiple thermal cycles and no actuation, the supports were changed to longer supports in hopes of increasing the spring tension. The supports were changed one more time with no noticeable difference to the load of the springs. The springs were removed and checked for any deformation. The springs were considerably deformed and were no longer capable of providing the needed pull force to actuate the device. New springs were acquired that would not deform as easily;

they are shown in figure 26. The new springs were chosen based on their spring constant, wire diameter, and maximum deflection and load.

Figure 26. Springs acquired after initial springs deformed. Top spring is Pt.#B6-50 and bottom spring is Pt.#80559S.

The springs were placed exactly as the other springs along with the longest supports. The first springs, Pt.#80559S, to be tested have an advertised spring constant of 6.6lbf/in and a maximum deflection of 1.5in. The switch was subjected to thermal cycling with small modifications to the spring stretched length. After three cycles, the magnets separated. Measurements were missed for this actuation. After this first actuation, the magnets were cooled quickly and tested again. The magnets separated at a temperature around 30°C. It is believed that the magnets actuated at such low temperature because they were not allowed to cool sufficiently and contained a lot of internal thermal energy. The magnets were tested two more times, after sufficient time to dissipate thermal energy, and actuated at temperatures around 70°C as expected. After it was shown that the springs will separate reliably around 70°C, it was needed to show that the magnets will re-actuate when allowed to cool on their own.

The switch was modified to allow a shorter distance between the magnets when separated. Upon the first trial, the epoxy between the top plate and top magnet broke. The top magnet needed to be re-epoxied before testing continued.

When re-epoxying the magnet it was noticed that the top magnets had surface damage, so it was replaced with a new magnet. The switch was again set up exactly the same way. The device was thermally cycled and re-adjusted acquire the desired spring length. After five cycles of unsuccessful trials, the springs were exchanged in favor of stiffer springs. These new springs, Pt.#B6-50, had a constant of 12lbf/in and maximum deflection of 0.940in. The device was cycled and re-adjusted. After successfully actuating the magnets once more, the magnets were allowed to cool for re-actuation.

The magnets did not re-actuate. It is believed that the brackets affected the magnetic field of the magnet. Bigger blocks of wood were place on the brackets to insulate the brackets from the magnets as seen above if figure 23. The device was heated up and the magnets manually separated. The magnets were allowed to cool to room temperature to observe the re-actuation. The gap closed once and upon further testing did not happen again. To prove the concept, the magnets were separated and allowed to come back together at room temperature. The magnets would not come back together if first heated and allowed to cool.

In order to separate the magnets when heated the magnets need to be a little stronger than when they are cooled. The threshold between to allow separation at high temperatures and closing at low temperatures is tiny. With the current equipment available, distances were not able to be set properly.

IX. Project Management Plan

The first quarter of the project was dedicated to research of relevant material such as existing products and novel materials. Design also started toward the end of the first quarter. Research was initially broad reviewing existing designs and finding new and exciting materials. As the design process started, research was narrowed to the information with more potential of developing a working prototype. At the end of the quarter, ferromagnets and SMAs held the most promise. There was also an interest in phase changing materials and gas conduction.

The second quarter consisted of refining the initial designs and completing the EES thermal analysis. Further research was conducted into the actual materials that would be used in the prototype and modeling of the heat path through the heat switch. Preliminary testing also started to test feasibility of the different actuation methods and materials to be used in the prototype. Neodymium magnets, nitinol springs, and Flexinol® Muscle Wire® were tested. The magnets were tested by heated by using a power resistor and a pull test to measure force. Both nitinol springs and Flexinol® needed power to actuate. Using the data collected a final design was chosen by the end of the quarter.

During the final quarter, a prototype was manufactured and tested for proof of concept. Final dimensions and fittings were decided before manufacturing started. The prototype was not a complete final product and was used and tested for proof of concept. Preliminary testing showed that the chosen actuation method is feasible and would make a good alternative to existing designs. Manufacturing had its difficulties because of tight tolerances. The springs need to be able to pull with enough force to separate the magnets at the desired temperature range but not too much that the magnetic force in the gap cannot overcome the same pull force when cooled.

X. Conclusion

After conducting and collecting experimental data for the two different actuation methods, SMAs and ferromagnets, the decision was made to move forward with ferromagnets for use in the final design. Magnets responded much better to the experimental tests, which lightly simulate the actual conditions that will be experienced in the device, and provided more reliable data as well as consistency. The SMAs did not react as well to the simulated condition, if at all, and failed to contract all but an extremely small amount even with direct heating at one end using a heat gun. Heat transfer occurred extremely slowly though the material which caused excruciatingly long actuation times as well as minimal contrition and force production.

A conceptual prototype was developed to test the actuation abilities of neodymium magnets in a similar orientation to that of the final design. Through multiple tests and various initial conditions, it was

proven that the reduction of magnetic force in the magnets is substantial enough to allow for actuation from the “ON” to “OFF” states. This actuation was repeated several times at each of the two operating conditions for which it occurred. Furthermore, at room temperature, when the magnets were manually changed from the “ON” state they would return on their own for extremely small “OFF” state gap distances. Returning the prototype to the “ON” state after heating however, posed several challenges and ultimately only occurred once during testing. Initially, the complications arose from the slight magnetic force between the brackets and actuating magnet. Although small pieces of wood lay in between the attraction was enough to restrict the magnets from reengaging. In order to mitigate this effect, larger pieces of wood were placed on top of the magnets. With this configuration, magnetic actuation back to the “ON” state did occur but was only proven once. Any slight nudge or movement would however, return the system from the “OFF” state to the “ON” state. Hence, the system was on the cusp between the two equilibrium points of the bi-stable system.

These results have proven that passive actuation using the temperature dependent magnetic properties of magnets is plausible for heat switch design. Although the results did not prove as repeatable as was expected, several factors and variations would allow for greater consistency when applied to a specific design. The gap distance between the magnets in the “OFF” state was the prominent variable and was extremely difficult to control given the capabilities of the prototype. Implementing brackets, which can be simultaneously adjusted, to provide the correct spacing to a high precision, such as by micrometers, would allow for the fine tuning necessary to establish the distances need for the bi-stable conditions of the system. Furthermore, higher strength mounting components and brackets would reduce the effects of deflection in the “OFF” state, maintaining the tight dimensions required. Additionally, the right spring force was highly important for obtaining actuation. Although the prototype did allow for slight adjustments of the spring length through the threaded attachments, providing for a more accurate way to adjust the stretched length along with more controllable gap distances would allow for far greater repeatability. When heating the magnets, applying a methodical heat source such as resistors, may also increase repeatability. Slower heat transfer rates would allow for heat dissipation to occur in a more uniform manner through the magnets, thus providing smaller temperature differences between them. As such, the magnetic fields would weaken at similar rates giving more stable and predictable actuation times.

When applying magnetic actuation to a cryogenic thermal switch several more recommendations should be noted. Steel was used in the prototype due to its availability and cost, but the complications due to the magnetic effects proved a challenge. Materials which do not exhibit these behaviors would serve far more reliable and mitigate any undesired magnetic effects. It should also be noted that the difference between the coefficient of thermal expansion of the magnets and material that it lays should be similar due to the range of temperature exposure. A mismatch could cause cracking or failure of the bonding agent which was seen in our tests when aluminum was used or the steel was heated very rapidly. Bi-metallic fixtures would prove another plausible remedy for this challenge. With regards to bonding itself, an agent proven at the desire temperature range is paramount. Epoxy failure compromises the performance of the entire system and cannot be easily remedied. Furthermore, implementing an epoxy with repeatable application thickness provides tighter control over the dimensions and subsequently the

gap distances. Machining and holding tighter tolerances and clearances is necessary for an actuation method as sensitive as this. Because the slightest variation could cause the system to fail to actuate, maintaining tolerances of only a few thousands of an inch is needed. Various types of magnets may be selected depending on the temperature range of the desired actuation. Testing was completed at atmospheric conditions, therefore neodymium magnets were used. For lower temperature in the cryogenic regime, magnets such as dysprosium and gadolinium should be considered. Further testing to determine the strength of their magnetic fields would need to be first conducted, and then a design point may be subsequently fashioned. Finally, investigating the possibility of adding a mechanical device to return the system from the "OFF" to "ON" states should considered. The slightest disturbance would provoke the system to return to the "ON" state, and through the use of temperature or remote control, the heat switch could be reengaged by an active system. Such a system may be considered if only for a failsafe situation.

Implementing magnets for use in cryogenic heat switches holds promise. Much research still needs to be conducted especially at those low temperatures to determine the magnetic force as a function of temperature. Once that information is obtained, specific design points can be established and consequently a unique design for a specific application.

With regards to the thermal requirements of the system, the model simulation carried out with EES demonstrates the designs fulfillment and potential. Using data obtained from experimental testing and geometries congruent with the prototype, conductance in the "ON" and "OFF" states was well as conductance ratios surpassed the required values. Since testing was only carried out to prove whether or not the actuation method was plausible, further thermal testing for a specific design catered to its particular application should also be completed. Preliminary computational analysis through thermal modeling for those specific geometries needs to be conducted prior to physical testing. Subsequently, the physic model developed from those results may be examined to obtain actual conductance values and ratios. Due to the small gap distances necessary to complete actuation to and from the "ON" to "OFF" states, radiative heat transfer in the "OFF" state may indeed prove a significant means of heat transfer and thus reduce the "OFF" state conductance as well as conductance ratio. Nevertheless, depending on the specific application and design criteria, a small increase in "OFF" state conduction may not hinder or compromise the heat switch. Furthermore, vacuum chamber testing may be required for certain applications in space environments.

Implementing magnets for use in cryogenic heat switches holds promise. Much research still needs to be conducted, especially at low temperatures in the cryogenic regime to determine the magnetic force as a function of temperature. Once that information is obtained, specific design points can be established and consequently a unique design for a specific application. Similarly, thermal data must be obtained to evaluate the overall performance of a heat switch in addition to its actuation capabilities. With further research, magnetic heat switches may provide a reliable alternative to the current methods available.

XI. References

1. *Cryogenics,* written by Michael McClintock, Reinhold Publishing Cooperation, 1964.
2. *Heat Transfer at Low Temperatures,* edited by Walter Frost, Plenum Press, New York and London, 1975.
3. Takashi Mineta, Yoichi Haga: Materials and Processes in Shape Memory Alloy, Graduate School of Science and Engineering, Yamagata University, Yonezawa, Japan (2011)
4. O. Haglund: Curie Temperature of Alloys, its Measurement and Technical Importance, Journal of Thermal Analysis, Vol. 25 (1982) 21-43
5. M. Prina, P. Bhandari, R. C. Bowman Jr., C. G. Paine, L. A. Wade: Development of Gas Gap Heat Switch Actuator for the Planck Sorption Cryocooler, Jet Propulsion Laboratory, Pasadena, CA, Politecnico di Milano, Milano, Italy
6. *Material Properties: G-10 CR (Fiberglass Epoxy)*, National Institute of Standards and Technology,
7. Binneberg A, Kaiser G, inventors; Oct. 23, 2001. Self-triggering cryogenic heat flow switch. United States patent US 6305174 B1
8. Stuart R, Hogan W, inventors; Mar. 4, 1969. Thermal Switch for Cryogenic Apparatus. United States patent US 3430455
9. Koichi Nishino, Shigemasa Yamashita, Kahoru Torii, Thermal contact conductance under low applied load in a vacuum environment, Experimental Thermal and Fluid Science, Volume 10, Issue 2, February 1995, Pages 258-271, ISSN 0894-1777, 10.1016/0894-1777(94)00091-L. (http://www.sciencedirect.com/science/article/pii/089417779400091L)
10. Mills, Anthony F. *Heat Transfer*. Upper Saddle River, NJ: Prentice Hall, 1999. Print.
11. T. McWaid, E. Marshall, Thermal contact resistance across pressed metal contacts in a vacuum environment, International Journal of Heat and Mass Transfer, Volume 35, Issue 11, November 1992, Pages 2911-2920, ISSN 0017-9310, 10.1016/0017-9310(92)90311-F. (http://www.sciencedirect.com/science/article/pii/001793109290311F)

XII. Appendices

A. Morphological Attributes List

IDEA GENERATION (Morphological Attributes)

Sys. Settings	Electrical	Detector/Sensor ~~H.T Mode~~	H.T Mode	Material	Mat'l Prop	Activation Sys	Heat Containment
Open ckt	Active	Solar Irradiation	Conduction	Metals	CTE	Piston (M)	Insulation
Closed ckt	Non-Active	T/C (ΔV) → PRT	Convection	Insulators	Conductance	Gap (P)	Wiring C
Ground		Set Cold Temp (To close ckt)	Radiation	Gases	Phase Change (P & T)	Wax (P)	Geometry
		Vaporization	- Natural	Composites	Geom. Structure	HXer (M)	Fins
		Thermostat	- Forced	Alloys	Heat Capacity	Evaporator (M)	Ground
		Magnetic Fields (Eddy Currents)		Plastics	Magnetism	Solar Array (E)	By-Pass
		Chemical Rxn		Carbon Based (Diamond)	Outgassing	Lever (M)	+ Pt. Contact
		Optics			Young's Modulus (E)	Diaphram (P)	
		Temp Gradient			Electrical Resistance	Pt. Contact (P)	
		Rotation			Emissivity	~~X~~ (View Factor)	
		Voltage			Transparent/translucent	Surface Area (Contact Area)	
		IR Sensors			~~Pressure~~	Geometry (△, ○, □)	
					~~Condensation~~	Chemical	
					€	Optics/Laser (Mirror)	
					+ Surface Finish (eg. paint, roughness)	Pressure	
						Condensation	
						Transition Lenses	
						Optics - Reflection Refraction	
						Combustion	
						+ Shells	
						+ Parabolic Fins	
						+ Shadow/Curtain	

Conservation of Mass
Conservation of Energy
H → C

CAME UP W/ IDEAS ~5 ON ENGR. PAPER 10/12/11

B. Conceptual Designs

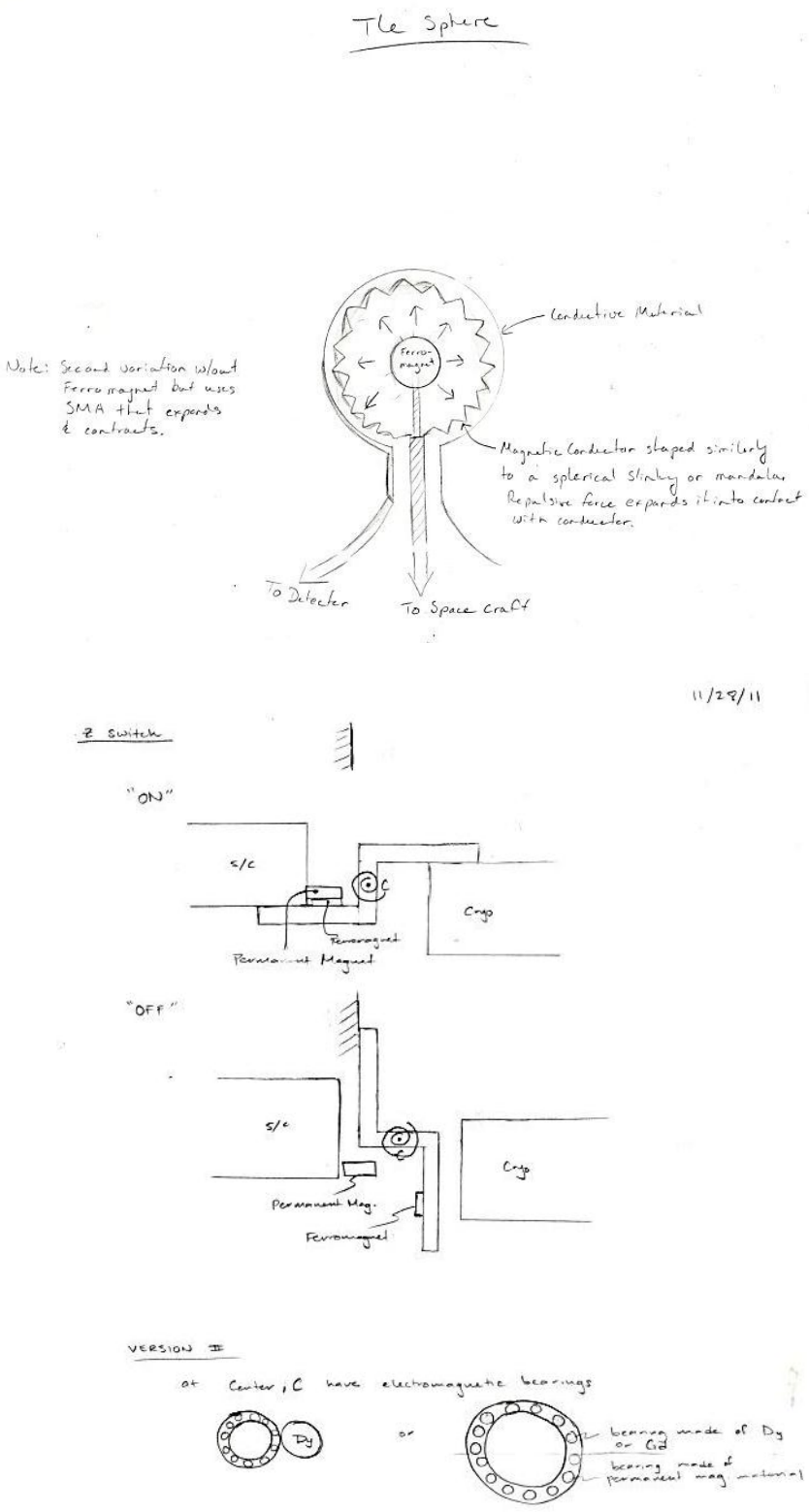

11/28/11

LIFT

"ON"

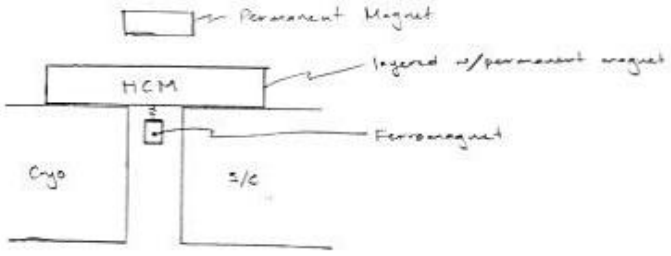

"OFF"

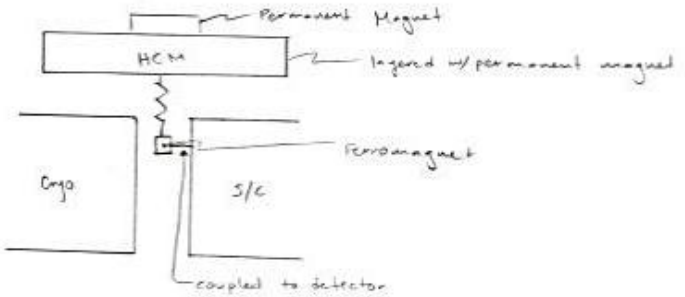

OFF

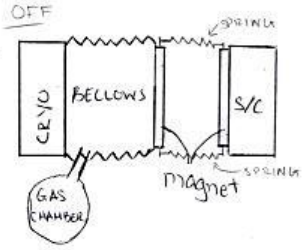

ON

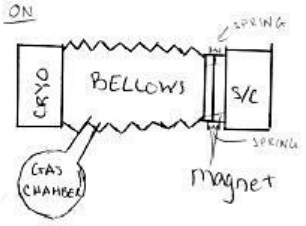

GAS CONDUCTANCE

NOTES:

- When ON, the bellow takes in gas from the gas chamber.
- When OFF, the gas is moved back to the gas chamber

FERLO – SPRING

OFF

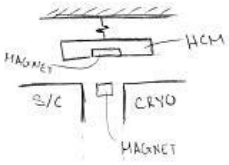

HCM = Highly Conductive Material

ON

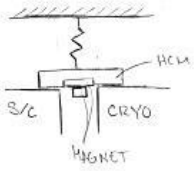

Domino

"OFF"

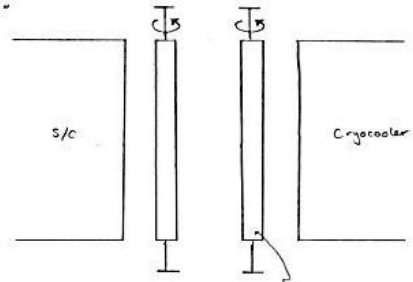

DOMINO (SEE BELOW)

"ON"

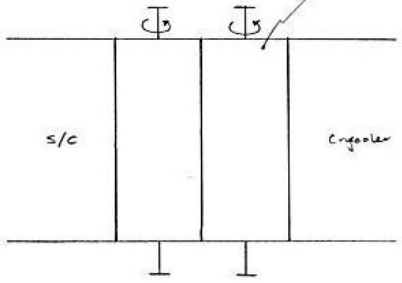

NOTES

- Can possibly be nanoscale
- Can have 1 Domino or multiple
  - if 1 Domino, we would have a magnetic material at the surface of the S/C & cryocooler

DOMINO

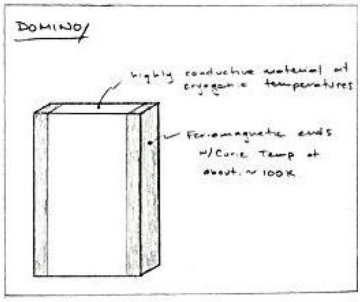

Gas diaphragm

ON

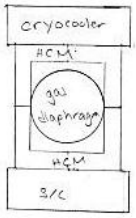

HCM= Highly conductive material

OFF

FERROMAGNETIC ROD

"OFF"

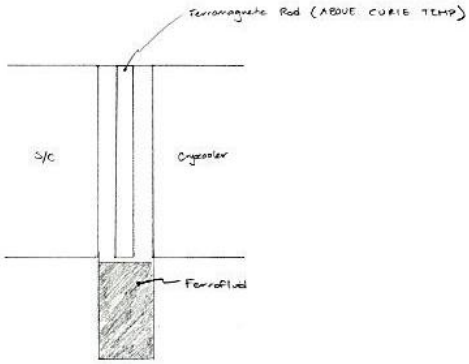

"ON"

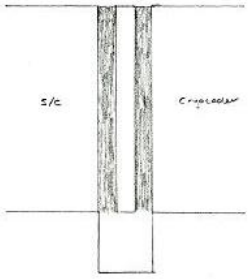

Linear Ferromagnetic Actuation

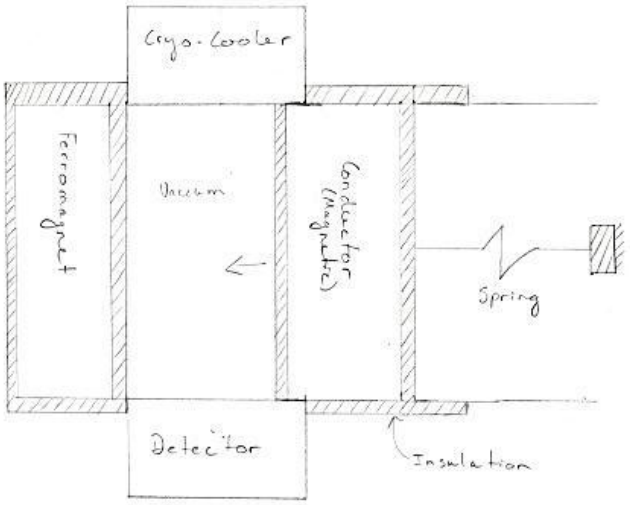

Note: Vacuum may be filled w/ conductive gas, while removing insulation on left side of conductor to help promote conduction across non-flat surfaces.

Ferromagnet with metal fillings

ON

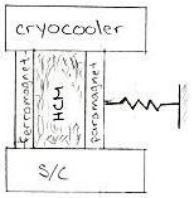

HCM = highly conductive material

NOTE:
The HCM could be metal shavings or an accordion style design

OFF

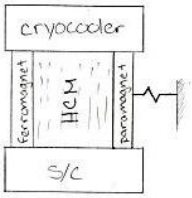

Shape memory alloy

ON

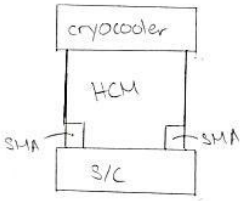

HCM = highly conductive material

SMA = shape memory alloy

OFF

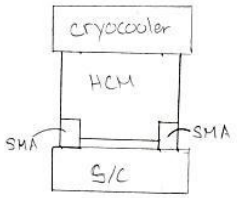

Rotary Ferromagnetic Actuation

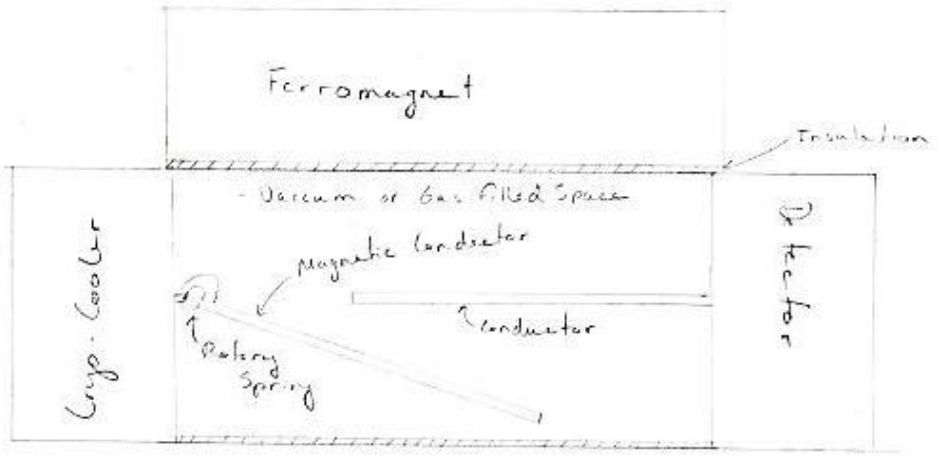

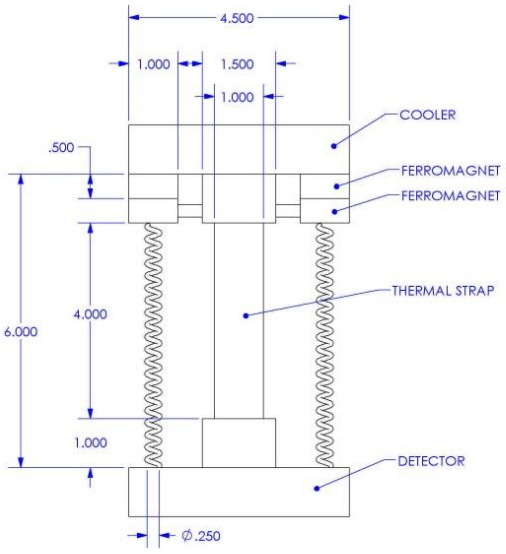

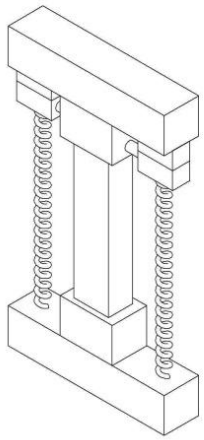

BOREAS	DATE: JAN. 17, 2012	UNITS: INCHES	MATERIAL:
	TOLERANCE:	SCALE: 1:2	TITLE: FM THERMAL STRAP
		NEXT ASSY:	NAME:
		DRAWING #:	SIGNATURE:

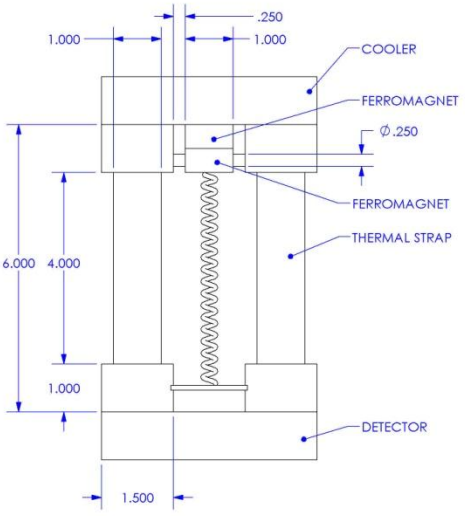

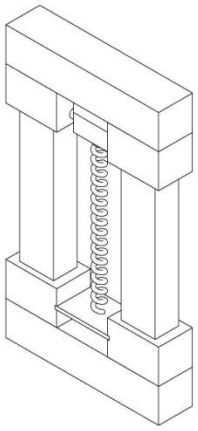

BOREAS	DATE: JAN. 17, 2012	UNITS: INCHES	MATERIAL:
	TOLERANCE:	SCALE: 1:2	TITLE: FM THERMAL SWITCH W/2TS
		NEXT ASSY:	NAME:
		DRAWING #:	SIGNATURE:

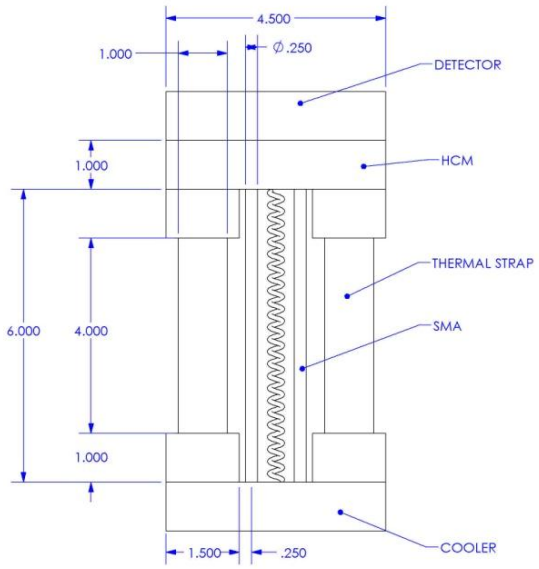

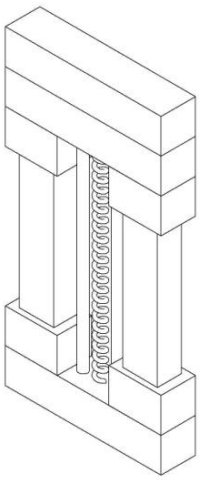

BOREAS	DATE: JAN. 17, 2012	UNITS: INCHES	MATERIAL:
	TOLERANCE:	SCALE: 1:2	TITLE: SMA THERMAL SWITCH
		NEXT ASSY:	NAME:
		DRAWING #:	SIGNATURE:

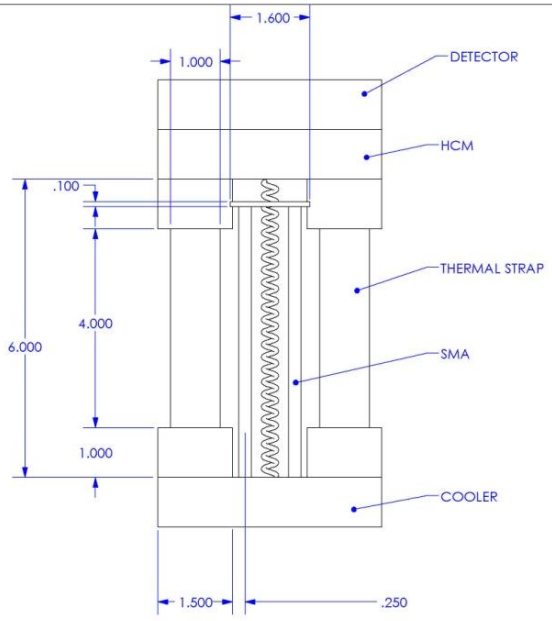

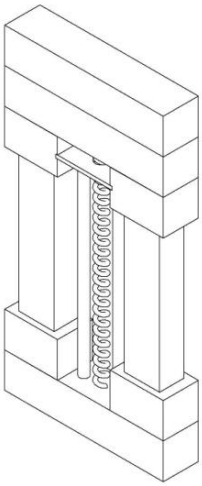

BOREAS	DATE: JAN. 17, 2012	UNITS: INCHES	MATERIAL:
	TOLERANCE:	SCALE: 1:2	TITLE: SMA THERMAL SWITCH DECOUPLED
		NEXT ASSY:	NAME:
		DRAWING #:	SIGNATURE:

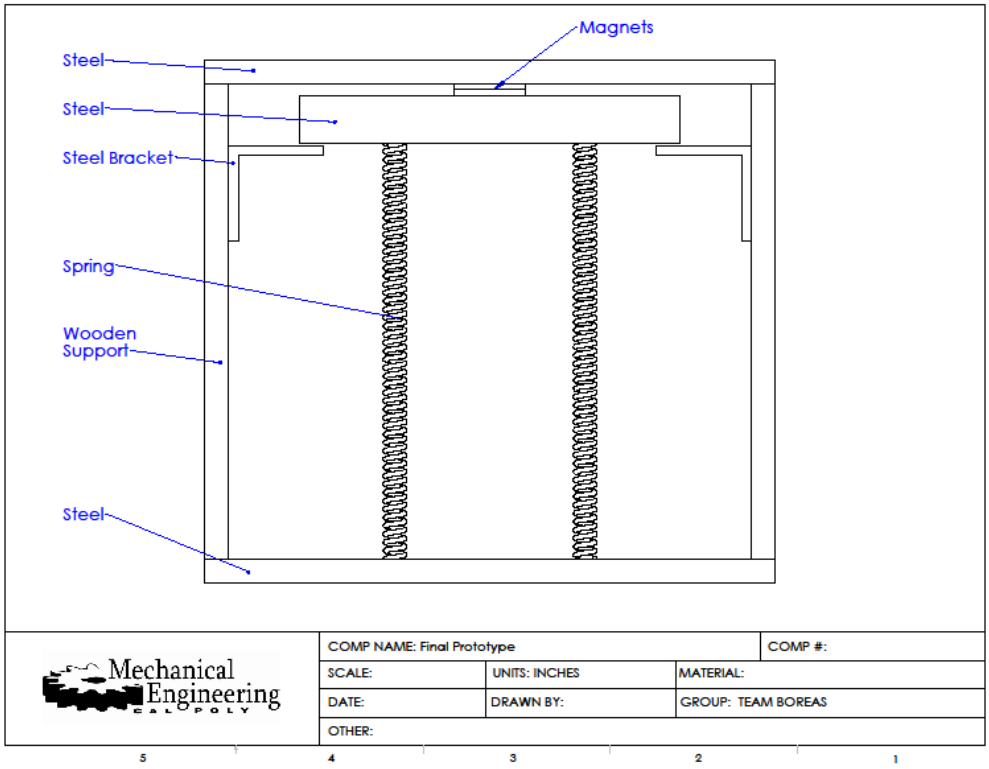

C. List of Vendors

Vendor Name	Material Supplied	Address	Phone Number	Email
K&J Magnetics	Ferromagnets		215-766-8055	contactus@kjmagnetics.com
Dynalloy, Inc.	Shape memory alloys	14762 Bentley Circle Tustin, CA 92780	714-436-1206	flexinol@dynalloy.com
DIGI-KEY	Power Resistor	701 Brooks Ave. S, Thief River Falls, MN 56701	800-344-4539	webmaster@digikey.com
ALS Group	Assorted Springs		888-992-5222	
Century Spring, Corp.	Assorted Springs	222 E. 16th Street, Los Angeles, CA 90015	213-749-1466	info@centuryspring.com

D. Vendor-Supplied Specifications and Data Sheets

Flexinol® Muscle Wire Properties

Properties — Flexinol name	025	037	050	075	100	125	150	200	250	300	375
Physical											
Wire Diameter (µm)	25	37	50	75	100	125	150	200	250	300	375
Minimum Bend Radius (mm)	1.3	1.85	2.5	3.75	5.0	6.25	7.5	10.0	12.50	15.0	18.75
Cross-sectional Area (µm²)	490	1,075	1,960	4,420	7,850	12,270	17,700	31,420	49,100	70,700	110,450
Electrical											
Linear Resistance (Ω/m)	1,770	860	510	200	150	70	50	31	20	13	8
Recommended Current# (mA)	20	30	50	100	180	250	400	610	1,000	1,750	2,750
Recommended Power# (W/m)	0.71	0.78	1.28	2.0	4.86	4.4	8.00	12.0	20.0	39.8	60.5
Strength*											
Max. Recovery Weight@600MPa(g)	29	65	117	250	469	736	1,056	1,860	2,933	4,240	6,630
Rec. Recovery Weight@190MPa (g)	7	20	35	80	150	230	330	590	930	1,250	2,000
Rec.Deformation Weight@35MPa(g)	2	4	8	815	28	43	62	110	172	245	393
Speed											
Typical Contraction Speed## (sec)	1.0	1.0	1.0	1.0	1.0	1.0	1.0	1.0	1.0	1.0	1.0
LT Relaxation Speed## (sec)	0.16	0.25	0.3	0.5	0.8	1.6	2.0	3.5	5.5	8.0	13.0
LT Alloy Thermal Cycle Rate (cyc/min)	52	48	46	40	33	23	20	13	9	7	4
HT Relaxation Speed## (sec)	n.a.		0.1	0.2	0.4	0.9	1.2	2.2	3.5	6	10
HT Alloy Thermal Cycle Rate (cyc/min)	n.a.	0.09	55	50	43	32	27	19	13	9	5
		55									

Thermal	*LT Alloy*	*HT Alloy*
Activation Start Temp. (°C)	68	88
Activation Finish Temp. (°C)	78	98
Relaxation Start Temp. (°C)	52	72
Relaxation Finish Temp. (°C)	42	62
Annealing Temp. (°C)	300	300
Melting Temp. (°C)	1,300	1,300
Specific Heat (cal/g°C)	0.077	0.077
Heat Capacity (Joule/g°C)	0.32	0.32
Latent Heat (Joule/g)	24.2	24.2

Material		
Density (g/cc)	6.45	
Maximum Recovery Force (MPa)	600	(~43 ton / in²)
Recommended Deformation Force (MPa)	35	(~2.5 ton / in²)
Breaking Strength (MPa)	1,000	(~71 ton / in²)
Poisson's Ratio	0.33	
Work Output (Joule/g)	1	
Energy Conversion Efficiency (%)	5	
Maximum Deformation Ratio (%)	8	
Recommended Deformation Ratio (%)	3-5	

Phase Related Phase	*Martensite*	*Austenite*
Resistivity (µΩcm)	76	82
Young's Modulus (GPa)	28	75
Magnetic Susceptibility (µemu/g)	2.5	3.8
Thermal Conductivity (W/cm°C)	0.08	0.18

† *In still air at 20°C* ++ *Depends greatly on local heating and cooling conditions.*

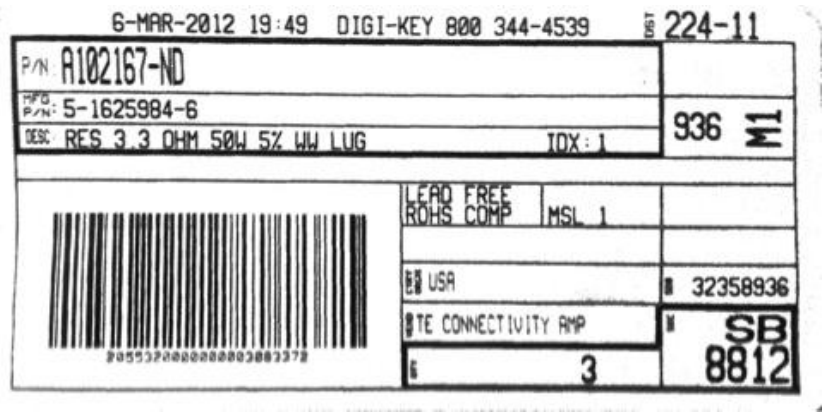

EXTENSION SPRING

Part Characteristics

CSC Stock #	80559S
OD (in)	0.359
Length (in)	2.750
Rate (lbs/in)	6.600
Initial Tension (lbs)	1.000
Sugg. Max Defl. (in)	1.500
Sugg. Max Load (lbs)	11.000
Wire Dia. (in)	0.052
Material	Stainless
Finish	None

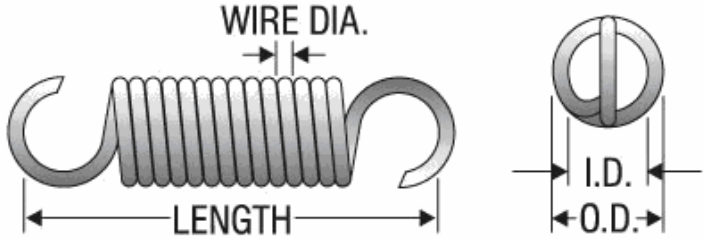

*NOTE: Image above is for reference only and not to scale.

Actual product may vary.

List Price: $7.89 Each

1 Add to Cart

EXTENSION SPRING

Part Characteristics

CSC Stock #	B6-50
OD (in)	0.359
Length (in)	2.250
Rate (lbs/in)	12.000
Initial Tension (lbs)	4.000
Sugg. Max Defl. (in)	0.940
Sugg. Max Load (lbs)	15.000
Wire Dia. (in)	0.054
Material	Spring Steel
Finish	None

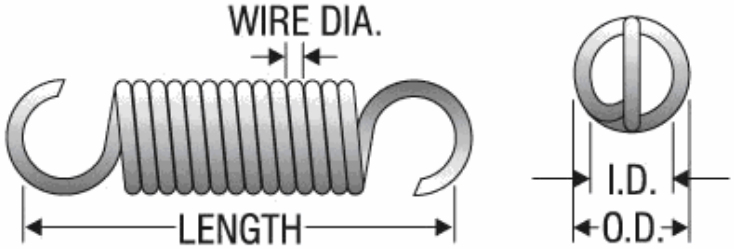

*NOTE: Image above is for reference only and not to scale.

Actual product may vary.

List Price: $1.87 Each

1 Add to Cart

E. EES Thermal Analysis

THERMAL CIRCUITS FOR ON STATE CONDUCTANCE

SMA CIRCUIT

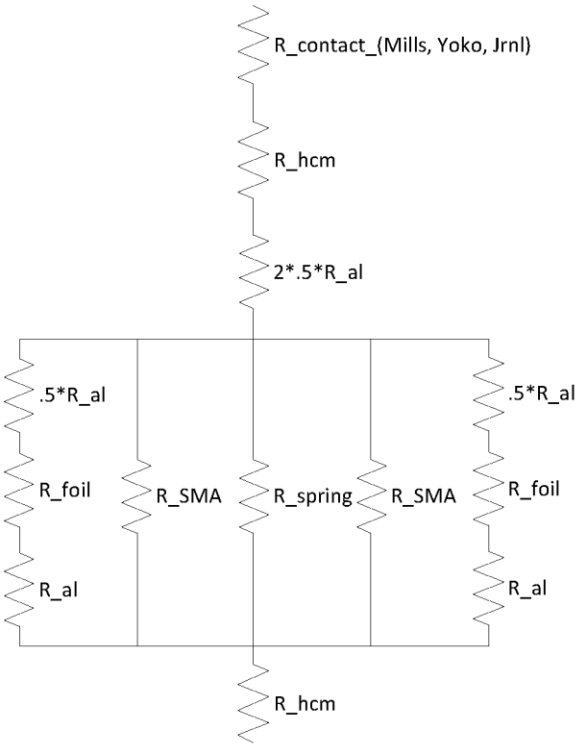

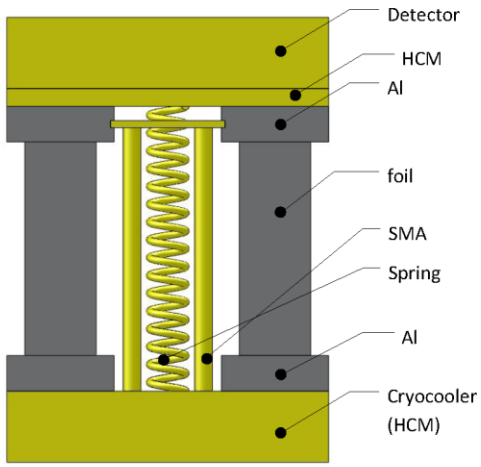

FM CIRCUIT

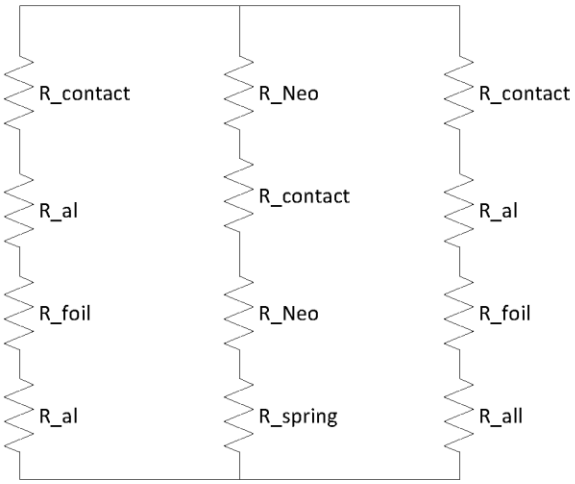

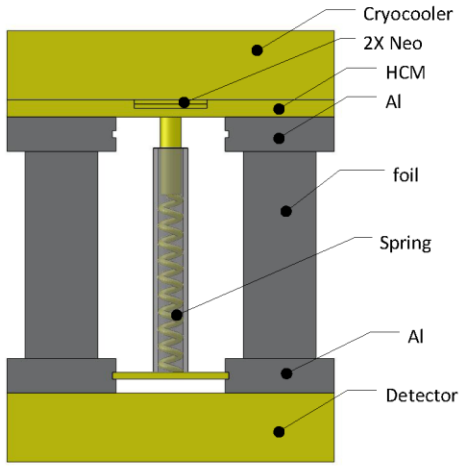

THERMAL CIRCUITS FOR OFF STATE CONDUCTANCE

SMA CIRCUIT-Pure Radiation

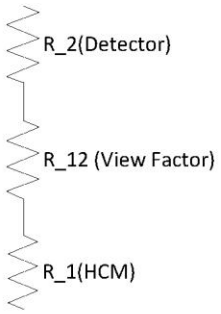

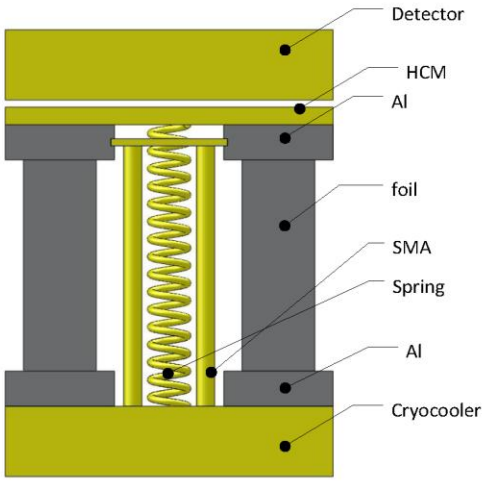

FM CIRCUIT-Pure Radiation

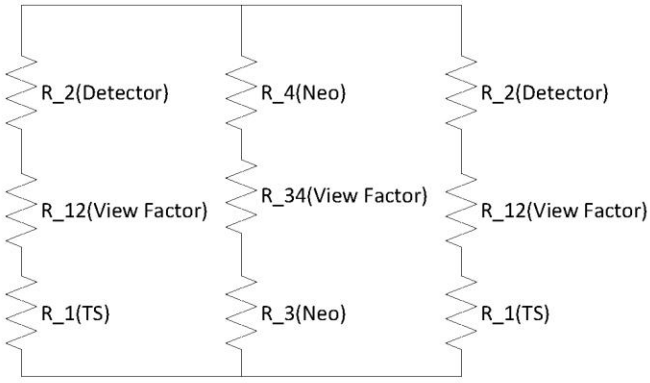

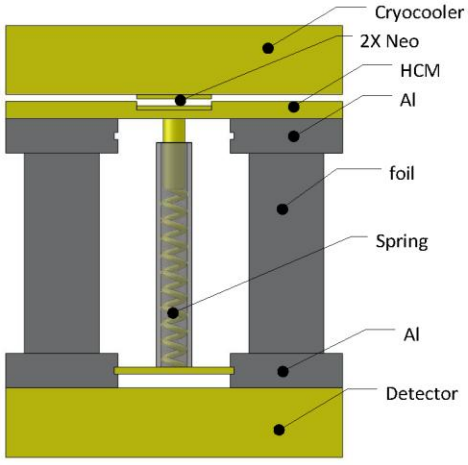

CONSTANTS(at 200k)

Pure Aluminum End Pieces

$k_{al} = 237$ [W/m*K]

$h_i = 150$ [W/m^2*K] *Rough Al- Al (Vacuum Conditions)- H.T Mills Text Estimate*

$F_{contact,lbf} = 7$ [lbf] *Update w/Tested values later*

$$P_{contact} = \frac{F_{contact,lbf}}{A_{al}} \cdot \left| 4.448222 \cdot \frac{N/cm^2}{lbf/cm^2} \right|$$

$$P_{contact,p} = P_{contact} \cdot \left| 1.45 \cdot \frac{lbf/in^2}{N/cm^2} \right|$$

Spring

$k_{sp} = 12.6$ [W/m*K] *Assuming stainless*

Neodymium

$k_{Neo} = 16.5$ [W/m*K] *Used Nickel*

Foils

$k_{foil} = 237$ [W/m*K]

Rod (Stainless AISI 304)

$k_{rod} = 12.6$ [W/m*K]

SMA-Nitinol Muscle Wire

$k_{sma} = 18$ [W/m*K] *from Dynalloy- for muscle wire*

Epoxy

$k_{epoxy} = 0.8$ [W/m*K] *Given by Keno*

GEOMETRIES

VERIFY ALL GEOMETRIES

Aluminum End Pieces

$L_{al} = 1 \cdot 2.54$ [cm] *length of heat path*

$t_{al} = 1 \cdot 2.54$ [cm]

$w_{al} = 1.5 \cdot 2.54$ [cm]

$A_{al} = t_{al} \cdot w_{al}$ *Increasing this Area will increase Conductance*

Spring

$L_{sp} = 6 \cdot 2.54$ [cm] *Rough Estimate- Full Body Length- length of heat path*

$D_{sp} = 0.1 \cdot 2.54$ [cm]

$A_{sp} = 3.14 \cdot \frac{D_{sp}^{2}}{4}$

Neodymium

$L_{Neo} = 0.5 \cdot 2.54$ [cm] *length of heat path*

$t_{Neo} = \frac{1}{16} \cdot 2.54$ [cm] *thickness is either 1/32 or 1/16 inch*

$w_{Neo} = 1.5 \cdot 2.54$ [cm]

$A_{Neo} = t_{Neo} \cdot w_{Neo}$

Foils

$L_{foil} = 4 \cdot 2.54$ [cm] *length of heat path*

$t_{foil} = 0.7 \cdot 2.54$ [cm] *total thickness of foils- not individual*

$w_{foil} = 1 \cdot 2.54$ [cm]

$A_{foil} = t_{foil} \cdot w_{foil}$ *Increasing this Area will increase Conductance*

HCM

$L_{hcm} = 1 \cdot 2.54$ [cm]

$t_{hcm} = 1 \cdot 2.54$ [cm]

$w_{hcm} = 4.5 \cdot 2.54$ [cm]

$A_{hcm} = t_{hcm} \cdot w_{hcm}$

SMA

$L_{sma} = 4 \cdot 2.54$ [cm]

$D_{sma} = 0.25 \cdot 2.54$ [cm]

$w_{sma} = 0.25 \cdot 2.54$ [cm]

$A_{sma} = 3.14 \cdot D_{sma}^{2}$

Epoxy

$t_{epoxy} = 0.005 \cdot 2.54$ [cm]

Thermal Equations

RESISTANCE

Aluminum End Pieces

$$R_{al} = L_{al} \cdot \frac{\left|0.01 \cdot \frac{m}{cm}\right|}{k_{al} \cdot A_{al} \cdot \left|0.0001 \cdot \frac{m^2}{cm^2}\right|}$$

Spring

$$R_{sp} = L_{sp} \cdot \frac{\left|0.01 \cdot \frac{m}{cm}\right|}{k_{sp} \cdot A_{sp} \cdot \left|0.0001 \cdot \frac{m^2}{cm^2}\right|}$$

Neodymium

$$R_{Neo} = L_{Neo} \cdot \frac{\left|0.01 \cdot \frac{m}{cm}\right|}{k_{Neo} \cdot A_{Neo} \cdot \left|0.0001 \cdot \frac{m^2}{cm^2}\right|}$$

SMA

$$R_{sma} = L_{sma} \cdot \frac{\left|0.01 \cdot \frac{m}{cm}\right|}{k_{sma} \cdot A_{sma} \cdot \left|0.0001 \cdot \frac{m^2}{cm^2}\right|}$$

Foils

$$R_{foil} = L_{foil} \cdot \frac{\left|0.01 \cdot \frac{m}{cm}\right|}{k_{foil} \cdot A_{foil} \cdot \left|0.0001 \cdot \frac{m^2}{cm^2}\right|}$$

HCM

$$R_{hcm} = L_{hcm} \cdot \frac{\left|0.01 \cdot \frac{m}{cm}\right|}{k_{al} \cdot A_{hcm} \cdot \left|0.0001 \cdot \frac{m^2}{cm^2}\right|}$$

Epoxy

$$R_{epoxy} = t_{epoxy} \cdot \frac{\left|0.01 \cdot \frac{m}{cm}\right|}{k_{epoxy} \cdot A_{Neo} \cdot \left|0.0001 \cdot \frac{m^2}{cm^2}\right|}$$

Contact- FM Area

$$R_{contact,Mills} = \frac{1}{h_i \cdot A_{al} \cdot \left| 0.0001 \cdot \frac{m^2}{cm^2} \right|}$$ *This is a rough estimate from H.T Mills text*

$$R_{contact,SW} = \frac{-0.0046 \cdot P_{contact} + 5.0465}{A_{al}}$$ *K=$_{cm2}$*K/W],This is the linear interpolation of the Solidworks table*

$$R_{contact,Yoko,fine} = \frac{100.78 \cdot P_{contact}^{-0.782}}{A_{al}}$$ *expK=$_{cm2}$*K/W],This is linear interpolation of a table in the journal*

$$R_{contact,Yoko,rough} = \frac{43.259 \cdot P_{contact}^{-0.427}}{A_{al}}$$ *expK=$_{cm2}$*K/W],This is linear interpolation of a table in the journal*

$$R_{contact,Jrnl,HT} = \frac{66.404 \cdot P_{contact}^{-0.72}}{A_{al}}$$ *expK=$_{cm2}$*K/W],This is linear interpolation of a table in the journal*

Contact- SMA Area

$$R_{scontact,Mills} = \frac{1}{h_i \cdot A_{hcm} \cdot \left| 0.0001 \cdot \frac{m^2}{cm^2} \right|}$$ *This is a rough estimate from H.T Mills text*

$$R_{scontact,SW} = \frac{-0.0046 \cdot P_{contact} + 5.0465}{A_{hcm}}$$

*K=$_{cm2}$*K/W],This is the linear interpolation of the Solidworks table*

$$R_{scontact,Yoko,fine} = \frac{100.78 \cdot P_{contact}^{-0.782}}{A_{hcm}}$$

*expK=$_{cm2}$*K/W],This is linear interpolation of a table in the journal*

$$R_{scontact,Yoko,rough} = \frac{43.259 \cdot P_{contact}^{-0.427}}{A_{hcm}}$$ *expK=$_{cm2}$*K/W],This is linear interpolation of a table in the jrnl*

$$R_{scontact,Jrnl,HT} = \frac{66.404 \cdot P_{contact}^{-0.72}}{A_{hcm}}$$ *expK=$_{cm2}$*K/W],This is linear interpolation of a table in the jrnl*

Thermal Circuits

FM Bottom Ckt Total

$$\frac{1}{R_{fm,bot}} = \frac{1}{R_{sp}} + \frac{1}{R_{al} + R_{foil} + R_{al}} + \frac{1}{R_{al} + R_{foil} + R_{al}}$$

FM Top Ckt Total

$$\frac{1}{R_{fm,top,Mills}} = \frac{1}{R_{contact,Mills} + 0.5 \cdot R_{hcm}} + \frac{1}{R_{epoxy} + R_{Neo} + R_{contact,Mills} + R_{Neo} + R_{epoxy}} + \frac{1}{R_{contact,Mills} + 0.5 \cdot R_{hcm}}$$

$$\frac{1}{R_{fm,top,SW}} = \frac{1}{R_{contact,SW} + 0.5 \cdot R_{hcm}} + \frac{1}{R_{epoxy} + R_{Neo} + R_{contact,SW} + R_{Neo} + R_{epoxy}} + \frac{1}{R_{contact,SW} + 0.5 \cdot R_{hcm}}$$

$$\frac{1}{R_{fm,top,Yoko,fine}} = \frac{1}{R_{contact,Yoko,fine} + 0.5 \cdot R_{hcm}} + \frac{1}{R_{epoxy} + R_{Neo} + R_{contact,Yoko,fine} + R_{Neo} + R_{epoxy}} + \frac{1}{R_{contact,Yoko,fine} + 0.5 \cdot R_{hcm}}$$

$$\frac{1}{R_{fm,top,Yoko,rough}} = \frac{1}{R_{contact,Yoko,rough} + 0.5 \cdot R_{hcm}} + \frac{1}{R_{epoxy} + R_{Neo} + R_{contact,Yoko,rough} + R_{Neo} + R_{epoxy}} + \frac{1}{R_{contact,Yoko,rough} + 0.5 \cdot R_{hcm}}$$

$$\frac{1}{R_{fm,top,Jml,HT}} = \frac{1}{R_{contact,Jml,HT} + 0.5 \cdot R_{hcm}} + \frac{1}{R_{epoxy} + R_{Neo} + R_{contact,Jml,HT} + R_{Neo} + R_{epoxy}} + \frac{1}{R_{contact,Jml,HT} + 0.5 \cdot R_{hcm}}$$

FM Total Thermal Circuit- ON State

$$R_{tot,fm,Mills} = R_{fm,top,Mills} + R_{fm,bot} + R_{hcm} + 0.5 \cdot R_{hcm}$$

$$R_{tot,fm,SW} = R_{fm,top,SW} + R_{fm,bot} + R_{hcm} + 0.5 \cdot R_{hcm}$$

$$R_{tot,fm,Yoko,fine} = R_{fm,top,Yoko,fine} + R_{fm,bot} + R_{hcm} + 0.5 \cdot R_{hcm}$$

$$R_{tot,fm,Yoko,rough} = R_{fm,top,Yoko,rough} + R_{fm,bot} + R_{hcm} + 0.5 \cdot R_{hcm}$$

$$R_{tot,fm,Jml,HT} = R_{fm,top,Jml,HT} + R_{fm,bot} + R_{hcm} + 0.5 \cdot R_{hcm}$$

SMA Bottom Ckt Total

$$\frac{1}{R_{sma,bot}} = \frac{1}{R_{sp}} + \frac{1}{R_{sma}} + \frac{1}{R_{sma}} + \frac{1}{1.5 \cdot R_{al} + R_{foil}} + \frac{1}{1.5 \cdot R_{al} + R_{foil}}$$

SMA Top Ckt Total

$$R_{sma,top,Mills} = R_{hcm} + R_{al} + R_{scontact,Mills}$$

$$R_{sma,top,SW} = R_{hcm} + R_{al} + R_{scontact,SW}$$

$$R_{sma,top,Yoko,fine} = R_{hcm} + R_{al} + R_{scontact,Yoko,fine}$$

$$R_{sma,top,Yoko,rough} = R_{hcm} + R_{al} + R_{scontact,Yoko,rough}$$

$$R_{sma,top,Jml,HT} = R_{hcm} + R_{al} + R_{scontact,Jml,HT}$$

SMA Total Thermal Ckt-ON State

$$R_{tot,sma,Mills} = R_{sma,bot} + R_{sma,top,Mills} + R_{hcm}$$

$$R_{tot,sma,SW} = R_{sma,bot} + R_{sma,top,SW} + R_{hcm}$$

$R_{tot,sma,Yoko,fine} = R_{sma,bot} + R_{sma,top,Yoko,fine} + R_{hcm}$

$R_{tot,sma,Yoko,rough} = R_{sma,bot} + R_{sma,top,Yoko,rough} + R_{hcm}$

$R_{tot,sma,Jml,HT} = R_{sma,bot} + R_{sma,top,Jml,HT} + R_{hcm}$

ON CONDUCTANCE

$$G_{tot,fm,Mills} = \frac{1}{R_{tot,fm,Mills}}$$

$$G_{tot,fm,SW} = \frac{1}{R_{tot,fm,SW}}$$

$$G_{tot,fm,Yoko,fine} = \frac{1}{R_{tot,fm,Yoko,fine}}$$

$$G_{tot,fm,Yoko,rough} = \frac{1}{R_{tot,fm,Yoko,rough}}$$

$$G_{tot,fm,Jml,HT} = \frac{1}{R_{tot,fm,Jml,HT}}$$

$$G_{tot,avg,fm} = \frac{G_{tot,fm,Mills} + G_{tot,fm,Yoko,fine} + G_{tot,fm,Yoko,rough} + G_{tot,fm,Jml,HT}}{4}$$

SW data excluded due to inconformity (outlier)

$$G_{tot,sma,Mills} = \frac{1}{R_{tot,sma,Mills}}$$

$$G_{tot,sma,SW} = \frac{1}{R_{tot,sma,SW}}$$

$$G_{tot,sma,Yoko,fine} = \frac{1}{R_{tot,sma,Yoko,fine}}$$

$$G_{tot,sma,Yoko,rough} = \frac{1}{R_{tot,sma,Yoko,rough}}$$

$$G_{tot,sma,Jml,HT} = \frac{1}{R_{tot,sma,Jml,HT}}$$

$$G_{tot,avg,sma} = \frac{G_{tot,sma,Mills} + G_{tot,sma,Yoko,fine} + G_{tot,sma,Yoko,rough} + G_{tot,sma,Jml,HT}}{4}$$

SW data excluded due to inconformity (outlier)

OFF CONDUCTANCE

View Factor

$t_{gap} = 0.1 \cdot 2.54$ [cm] *Parametric Table completed*

$e_1 = 0.19$ [-] *emissivity for Al oxidized*

$e_2 = 0.19$ [-] *emissivity for Al oxidized*

$F_{12} = 1$ *assume 1 for 2 parallel inf. long flat plates*

Radiation

$T_s = 40$ [K] *Temperature of the surface aka temperature of detector*

$T_{sur} = 293$ [K]

Temperature of the surrounding aka temperature of cryocooler varies from 20K to 293K (worse case Tsun)

$sig = 5.678 \times 10^{-8}$ [W/m^2*K^4]

FM Radiation Resistance

$$X = \frac{w_{al}}{t_{gap}}$$

$$Y = \frac{t_{al}}{t_{gap}}$$

$e_3 = 0.36$ [-] *emissivity for Ni oxidized- engineering toolbox(high)*

$e_4 = 0.36$ [-] *emissivity for Ni oxidized- engineering toolbox(high)*

$$X_n = \frac{w_{Neo}}{t_{gap}}$$

$$Y_n = \frac{t_{Neo}}{t_{gap}}$$

$F_{34} = 1$ *assume 1 for 2 parallel inf. long flat plates*

$$R_1 = \frac{1 - e_1}{e_1 \cdot A_{al} \cdot \left| 0.0001 \cdot \frac{m^2}{cm^2} \right|}$$ *Thermal Strap*

$$R_2 = \frac{1 - e_2}{e_2 \cdot A_{al} \cdot \left| 0.0001 \cdot \frac{m^2}{cm^2} \right|}$$ *Detector Side*

$$R_{12} = \frac{1}{A_{al} \cdot \left| 0.0001 \cdot \frac{m^2}{cm^2} \right| \cdot F_{12}}$$ *View Factor*

$$R_3 = \frac{1 - e_3}{e_3 \cdot A_{Neo} \cdot \left| 0.0001 \cdot \frac{m^2}{cm^2} \right|}$$ *Thermal Strap*

$$R_4 = \frac{1 - e_4}{e_4 \cdot A_{Neo} \cdot \left| 0.0001 \cdot \frac{m^2}{cm^2} \right|}$$ *Detector Side*

$$R_{34} = \frac{1}{A_{Neo} \cdot \left| 0.0001 \cdot \frac{m^2}{cm^2} \right| \cdot F_{34}}$$ *View Factor*

$$\frac{1}{R_{14}} = \frac{1}{R_1 + R_{12} + R_2} + \frac{1}{R_3 + R_{34} + R_4} + \frac{1}{R_1 + R_{12} + R_2}$$ *Total Resistance for fm*

$$Q_{14} = \frac{sig \cdot \left[T_{sur}^{\ 4} - T_s^{\ 4} \right]}{R_{14}}$$

$$R_{rad,fm,gap} = \frac{T_{sur} - T_s}{Q_{14}}$$ *linearization of resistance for FM*

$$\frac{1}{R_{fm,top}} = \frac{1}{0.5 \cdot R_{hcm}} + \frac{1}{R_{epoxy} + R_{Neo} + R_{Neo} + R_{epoxy}} + \frac{1}{0.5 \cdot R_{hcm}}$$

$$R_{off,fm} = R_{rad,fm,gap} + R_{fm,bot} + R_{hcm} + 0.5 \cdot R_{hcm} + R_{fm,top}$$

SMA Radiation Resistance

$F_{12s} = 1$ *assume 1 for 2 parallel inf. long flat plates*

$$X_s = \frac{w_{hcm}}{t_{gap}}$$

$$Y_s = \frac{t_{hcm}}{t_{gap}}$$

$$R_{1s} = \frac{1 - e_1}{e_1 \cdot A_{hcm} \cdot \left| 0.0001 \cdot \frac{m^2}{cm^2} \right|}$$ *Thermal Strap*

$$R_{2s} = \frac{1 - e_2}{e_2 \cdot A_{hcm} \cdot \left| 0.0001 \cdot \frac{m^2}{cm^2} \right|}$$ *Detector Side*

$$R_{12s} = \frac{1}{A_{hcm} \cdot \left| 0.0001 \cdot \frac{m^2}{cm^2} \right| \cdot F_{12s}}$$ *View Factor*

$$Q_{12} = \frac{sig \cdot \left[T_{sur}^{\ 4} - T_s^{\ 4} \right]}{R_{1s} + R_{12s} + R_{2s}}$$

$$R_{rad,sma,gap} = \frac{T_{sur} - T_s}{Q_{12}}$$ *linearization of resistance for SMA*

$$R_{off,sma} = R_{rad,sma,gap} + R_{hcm} + R_{sma,bot} + R_{hcm} + R_{al}$$

OFF State Conduction for atmospheric testing for FM and SMA

$k_{air} = 0.0285$ [W/m*K] *at 60 deg.C- engineering toolbox atm press.*

$$\frac{1}{R_{cond,fm,gap}} = \left[\frac{1}{\frac{t_{gap}}{k_{air} \cdot A_{al}}} + \frac{1}{\frac{t_{gap}}{k_{air} \cdot A_{al}}} + \frac{1}{\frac{t_{gap}}{k_{air} \cdot A_{Neo}}} \right] \cdot \left| 0.0001 \cdot \frac{m^2}{cm^2} \right| \cdot \frac{1}{\left| 0.01 \cdot \frac{m}{cm} \right|}$$ *Resistance due*

to conduction

$$R_{cond,sma,gap} = \frac{t_{gap} \cdot \left| 0.01 \cdot \frac{m}{cm} \right|}{k_{air} \cdot A_{hcm} \cdot \left| 0.0001 \cdot \frac{m^2}{cm^2} \right|}$$ *Resistance due to conduction*

OFF State Conduction and Radiation for FM and SMA

$$\frac{1}{R_{off,fm,stp}} = \frac{1}{R_{rad,fm,gap}} + \frac{1}{R_{cond,fm,gap}}$$

Total Resistance due to radiation and conduction act in parallel

$$\frac{1}{R_{off,sma,stp}} = \frac{1}{R_{rad,sma,gap}} + \frac{1}{R_{cond,sma,gap}}$$ *Total Resistance due to radiation and conduction act in parallel*

Pure Radiation Conductance in OFF State

$$G_{off,fm} = \frac{1}{R_{off,fm}}$$ *Total Conductance due to radiation*

$$G_{off,sma} = \frac{1}{R_{off,sma}}$$ *Total Conductance due to radiation*

Radiation and Conduction Conductance in OFF State- for STP testing

$$G_{off,fm,stp} = \frac{1}{R_{off,fm,stp}}$$ *Total Conductance due to radiation and conduction*

$$G_{off,sma,stp} = \frac{1}{R_{off,sma,stp}}$$ *Total Conductance due to radiation and conduction*

ON/OFF Ratios

NOTE: (Off = Radiation Only)

$$Ratio_{fm} = \frac{G_{tot,avg,fm}}{G_{off,fm}}$$

$$Ratio_{sma} = \frac{G_{tot,avg,sma}}{G_{off,sma}}$$

SOLUTION

Unit Settings: SI C kPa kJ mass deg

A_{al} = 9.677 [cm^2]
A_{foil} = 4.516 [cm^2]
A_{hcm} = 29.03 [cm^2]
A_{Neo} = 0.6048 [cm^2]
A_{sma} = 1.266 [cm^2]
A_{sp} = 0.05065 [cm^2]
D_{sma} = 0.635 [cm]
D_{sp} = 0.254 [cm]

e_1 = 0.19 [-]
e_2 = 0.19 [-]
e_3 = 0.36 [-]
e_4 = 0.36 [-]
F_{12} = 1 [-]
F_{12s} = 1 [-]
F_{34} = 1 [-]
$F_{contact,lbf}$ = 7 [lbf]
$G_{off,fm}$ = 0.0003578
$G_{off,fm,stp}$ = 0.02275
$G_{off,sma}$ = 0.0005037
$G_{off,sma,stp}$ = 0.03308
$G_{tot,avg,fm}$ = 0.4102 [W/K]
$G_{tot,avg,sma}$ = 0.4994 [W/K]
$G_{tot,fm,Jrnl,HT}$ = 0.4841 [W/K]
$G_{tot,fm,Mills}$ = 0.2629 [W/K]
$G_{tot,fm,SW}$ = 1.102 [W/K]
$G_{tot,fm,Yoko,fine}$ = 0.3819 [W/K]
$G_{tot,fm,Yoko,rough}$ = 0.512 [W/K]
$G_{tot,sma,Jrnl,HT}$ = 0.5832 [W/K]
$G_{tot,sma,Mills}$ = 0.3306 [W/K]
$G_{tot,sma,SW}$ = 1.109 [W/K]
$G_{tot,sma,Yoko,fine}$ = 0.4716 [W/K]
$G_{tot,sma,Yoko,rough}$ = 0.6123 [W/K]
h_i = 150 [W/m^2*K]
k_{air} = 0.0285 [W/m*K]
k_{al} = 237 [W/m*K]
k_{epoxy} = 0.8 [W/m*K]
k_{foil} = 237 [W/m*K]
k_{Neo} = 16.5 [W/m*K]
k_{rod} = 12.6 [W/m*K]
k_{sma} = 18 [W/m*K]
k_{sp} = 12.6 [W/m*K]
L_{al} = 2.54 [cm]
L_{foil} = 10.16 [cm]
L_{hcm} = 2.54 [cm]
L_{Neo} = 1.27 [cm]
L_{sma} = 10.16 [cm]
L_{sp} = 15.24 [cm]
$P_{contact}$ = 3.218 [N/cm^2]
$P_{contact,p}$ = 4.667 [lbf/in^2]
Q_{12} = 0.1275 [W]
Q_{14} = 0.09055 [W]
$Ratio_{fm}$ = 1146 [-]
$Ratio_{sma}$ = 991.5 [-]
R_1 = 4405 [m^{-2}]
R_{12} = 1033 [m^{-2}]
R_{12s} = 344.4 [m^{-2}]
R_{14} = 4620 [m^{-2}]
R_{1s} = 1468 [m^{-2}]
R_2 = 4405 [m^{-2}]
R_{2s} = 1468 [m^{-2}]
R_3 = 29393 [m^{-2}]
R_{34} = 16533 [m^{-2}]
R_4 = 29393 [m^{-2}]

$R_{al} = 0.1107$ [K/W]
$R_{cond,fm,gap} = 44.65$
$R_{cond,sma,gap} = 30.7$
$R_{contact,Jrnl,HT} = 2.958$ [K/W]
$R_{contact,Mills} = 6.889$ [K/W]
$R_{contact,SW} = 0.5199$ [K/W]
$R_{contact,Yoko,fine} = 4.176$ [K/W]
$R_{contact,Yoko,rough} = 2.714$ [K/W]
$R_{epoxy} = 2.625$ [K/W]
$R_{fm,bot} = 0.5852$ [K/W]
$R_{fm,top} = 0.009226$
$R_{fm,top,Jrnl,HT} = 1.425$ [K/W]
$R_{fm,top,Mills} = 3.163$ [K/W]
$R_{fm,top,SW} = 0.2669$ [K/W]
$R_{fm,top,Yoko,fine} = 1.978$ [K/W]
$R_{fm,top,Yoko,rough} = 1.313$ [K/W]
$R_{foil} = 0.9492$ [K/W]
$R_{hcm} = 0.03692$ [K/W]
$R_{Neo} = 12.73$ [K/W]
$R_{off,fm} = 2795$
$R_{off,fm,stp} = 43.95$
$R_{off,sma} = 1985$
$R_{off,sma,stp} = 30.23$
$R_{rad,fm,gap} = 2794$
$R_{rad,sma,gap} = 1984$
$R_{scontact,Jrnl,HT} = 0.986$ [K/W]
$R_{scontact,Mills} = 2.296$ [K/W]
$R_{scontact,SW} = 0.1733$ [K/W]
$R_{scontact,Yoko,fine} = 1.392$ [K/W]
$R_{scontact,Yoko,rough} = 0.9047$ [K/W]
$R_{sma} = 44.58$ [K/W]
$R_{sma,bot} = 0.5439$ [K/W]
$R_{sma,top,Jrnl,HT} = 1.134$ [K/W]
$R_{sma,top,Mills} = 2.444$ [K/W]
$R_{sma,top,SW} = 0.321$ [K/W]
$R_{sma,top,Yoko,fine} = 1.54$ [K/W]
$R_{sma,top,Yoko,rough} = 1.052$ [K/W]
$R_{sp} = 2388$ [K/W]
$R_{tot,fm,Jrnl,HT} = 2.066$ [K/W]
$R_{tot,fm,Mills} = 3.804$ [K/W]
$R_{tot,fm,SW} = 0.9075$ [K/W]
$R_{tot,fm,Yoko,fine} = 2.619$ [K/W]
$R_{tot,fm,Yoko,rough} = 1.953$ [K/W]
$R_{tot,sma,Jrnl,HT} = 1.715$ [K/W]
$R_{tot,sma,Mills} = 3.025$ [K/W]
$R_{tot,sma,SW} = 0.9018$ [K/W]
$R_{tot,sma,Yoko,fine} = 2.12$ [K/W]
$R_{tot,sma,Yoko,rough} = 1.633$ [K/W]
$sig = 5.678E-08$ [W/m^2*K^4]
$t_{al} = 2.54$ [cm]
$t_{epoxy} = 0.0127$ [cm]
$t_{foil} = 1.778$ [cm]
$t_{gap} = 0.254$ [cm]
$t_{hcm} = 2.54$ [cm]
$t_{Neo} = 0.1588$ [cm]

T_s = 40 [K]
T_{sur} = 293 [K]
w_{al} = 3.81 [cm]
w_{foil} = 2.54 [cm]
w_{hcm} = 11.43 [cm]
w_{Neo} = 3.81 [cm]
w_{sma} = 0.635 [cm]
X = 15 [-]
X_n = 15 [-]
X_s = 45 [-]
Y = 10 [-]
Y_n = 0.625 [-]
Y_s = 10 [-]

17 potential unit problems were detected.

F. Gantt Chart

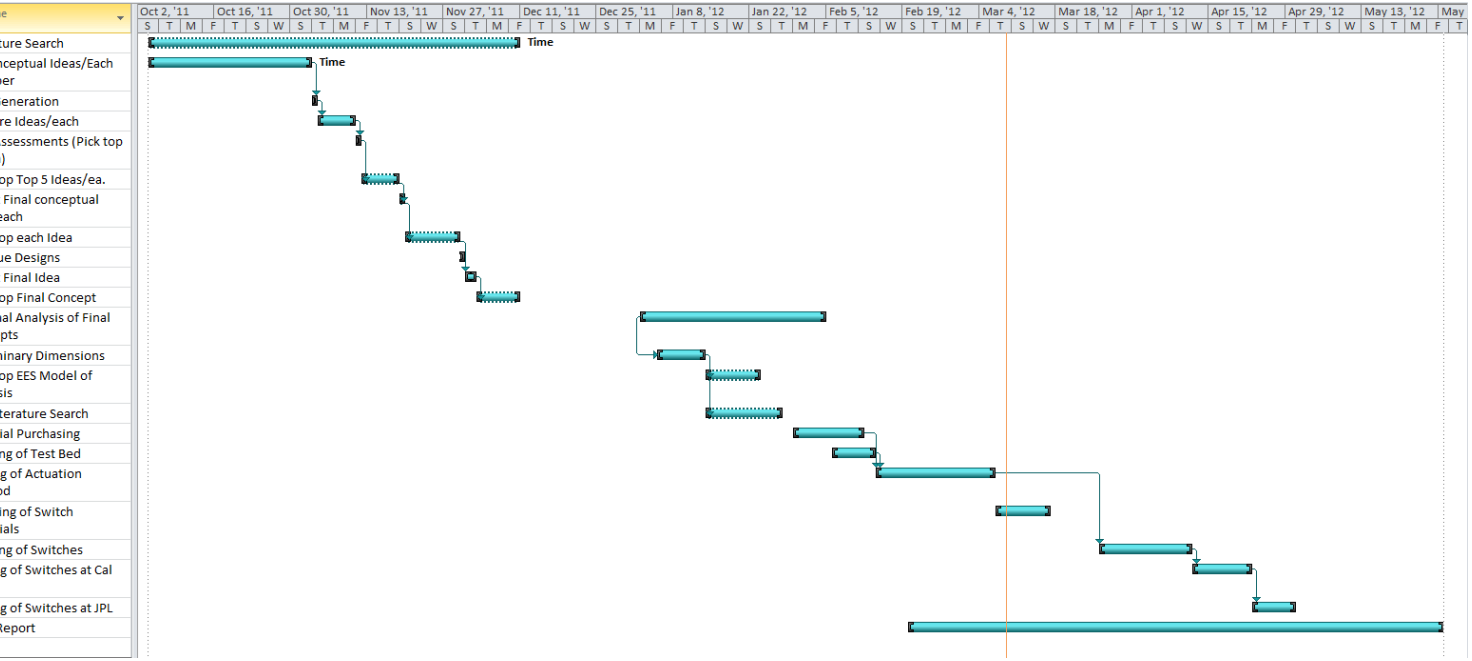
ture Search
nceptual Ideas/Each
ber
eneration
re Ideas/each
ssessments (Pick top
)
op Top 5 Ideas/ea.
Final conceptual
each
op each Idea
ue Designs
Final Idea
op Final Concept
al Analysis of Final
pts
inary Dimensions
op EES Model of
sis
terature Search
ial Purchasing
ng of Test Bed
g of Actuation
od
ing of Switch
ials
ng of Switches
g of Switches at Cal
g of Switches at JPL
Report
Oct 2, '11
Oct 16, '11
Oct 30, '11
Nov 13, '11
Nov 27, '11
Dec 11, '11
Dec 25, '11
Jan 8, '12
Jan 22, '12
Feb 5, '12
Feb 19, '12
Mar 4, '12
Mar 18, '12
Apr 1, '12
Apr 15, '12
Apr 29, '12
May 13, '12
May
Time
Time

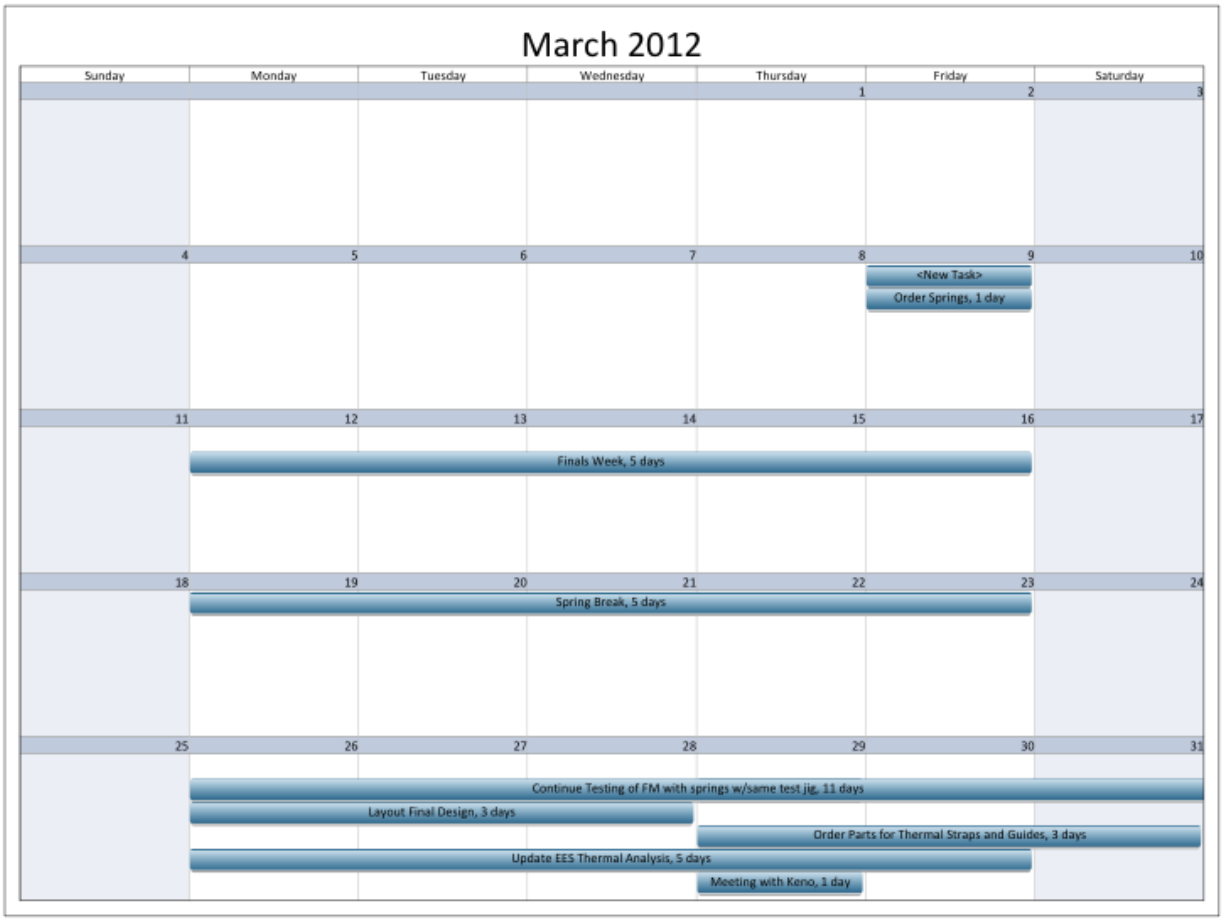
March 2012
Sunday
Monday
Tuesday
Wednesday
Thursday
Friday
Saturday
1
2
3
4
5
6
7
8
9
10
<New Task>
Order Springs, 1 day
11
12
13
14
15
16
17
Finals Week, 5 days
18
19
20
21
22
23
24
Spring Break, 5 days
25
26
27
28
29
30
31
Continue Testing of FM with springs w/same test jig, 11 days
Layout Final Design, 3 days
Order Parts for Thermal Straps and Guides, 3 days
Update EES Thermal Analysis, 5 days
Meeting with Keno, 1 day

April 2012

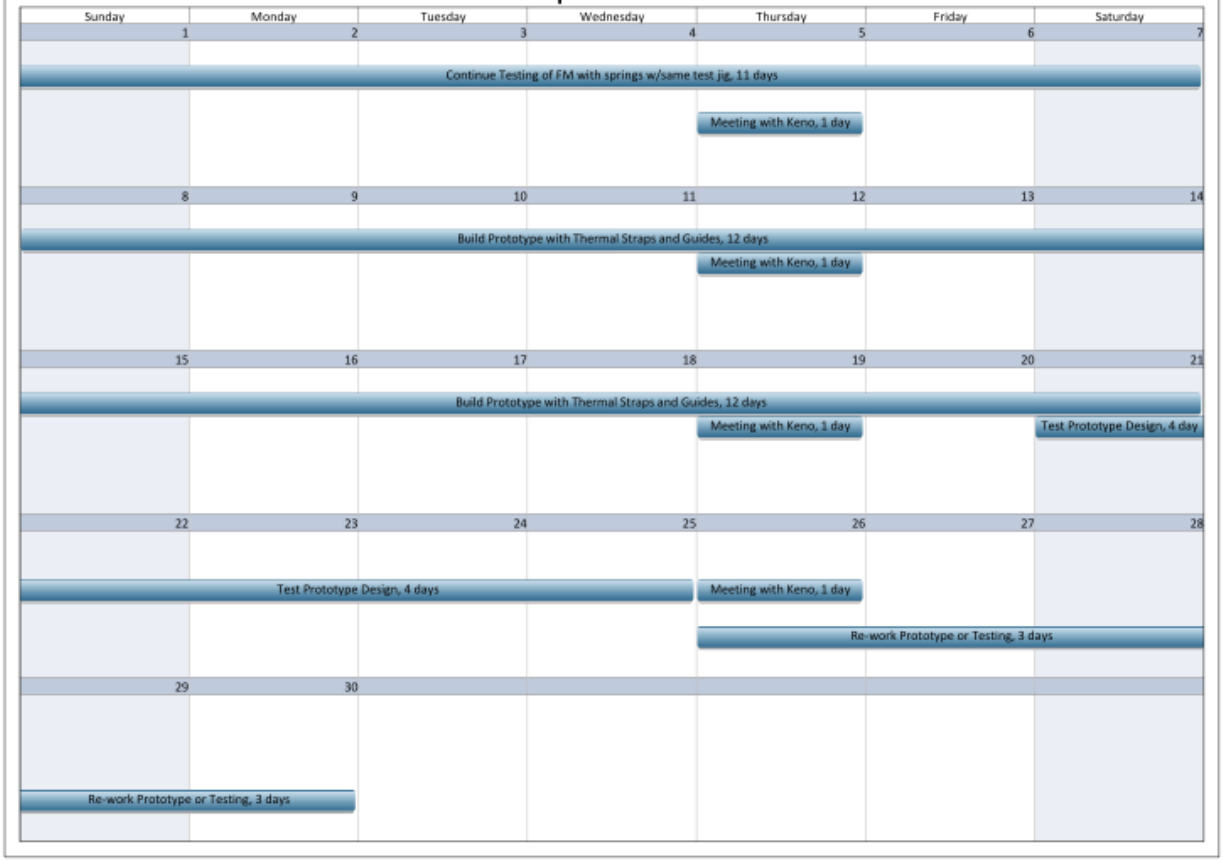
Sunday
Monday
Tuesday
Wednesday
Thursday
Friday
Saturday
1
2
3
4
5
6
7
Continue Testing of FM with springs w/same test jig, 11 days
Meeting with Keno, 1 day
8
9
10
11
12
13
14
Build Prototype with Thermal Straps and Guides, 12 days
Meeting with Keno, 1 day
15
16
17
18
19
20
21
Build Prototype with Thermal Straps and Guides, 12 days
Meeting with Keno, 1 day
Test Prototype Design, 4 day
22
23
24
25
26
27
28
Test Prototype Design, 4 days
Meeting with Keno, 1 day
Re-work Prototype or Testing, 3 days
29
30
Re-work Prototype or Testing, 3 days

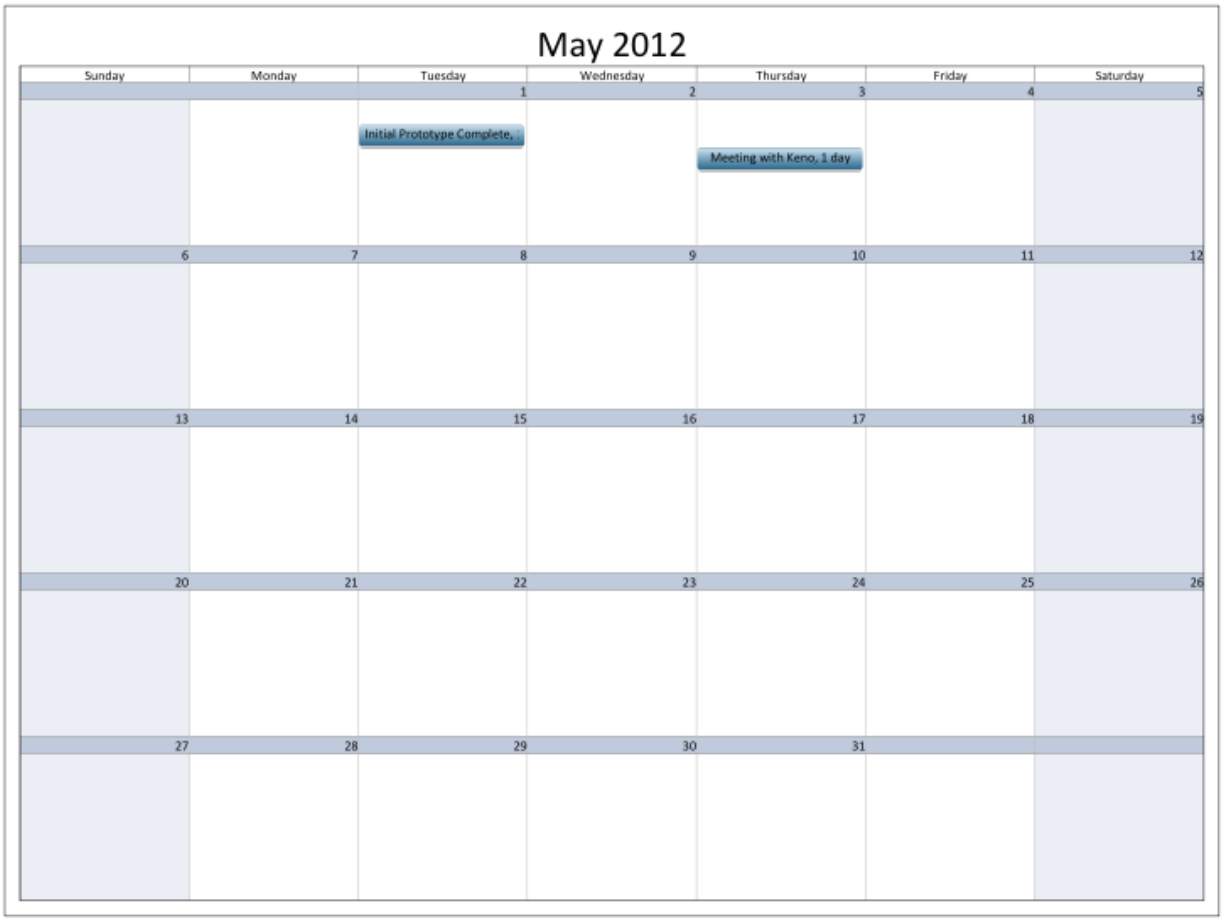

G. Test Equipment

Equipment	Brand	Model #
Power Source	Agilent Technologies	N5747A
Thermocouple Reader	OMEGA®	HH23
Force Gauge	Cen-Tech®	97227
Heat Gun	Masterflow®	AH-501

XIII. Acknowledgements

Eugenio Urquiza, Jet Propulsion Laboratory mentor

Jose I. Rodriguez, Jet Propulsion Laboratory advisor

Paige Lewis, Cryoquip technical advisor - discussed cryogenics and properties of gases

Mohammad Noori, Senior project advisor